The FEBS Journal

FEBS PRESS science publishing by scientists

Structure-based design, synthesis and biological evaluation of a NAD^+ analogue targeting *Pseudomonas aeruginosa* NAD kinase

Rahila Rahimova[1], Pauline Nogaret[2], Valérie Huteau[3], Muriel Gelin[1], David A. Clément[3], Gilles Labesse[1], Sylvie Pochet[3], Anne-Béatrice Blanc-Potard[2] and Corinne Lionne[1]

1 Centre de Biologie Structurale (CBS), Université de Montpellier, CNRS UMR 5048, INSERM U1054, France
2 Laboratory of Pathogen Host Interactions (LPHI), Université de Montpellier, CNRS UMR 5235, France
3 Unité de Chimie Biologique Epigénétique, Institut Pasteur, Université Paris Cité, CNRS UMR3523, France

Keywords
antibiotics; benzamide adenine dinucleoside analogue; ESKAPE; new target enzyme; zebrafish

Correspondence
S. Pochet, Unité de Chimie Biologique Epigénétique, Institut Pasteur, Université Paris Cité, CNRS UMR3523, 28 rue du Dr Roux, F-75015 Paris, France
Tel: +33 140 613 805
E-mail: sylvie.pochet@pasteur.frA. Blanc-Potard, Laboratory of Pathogen Host Interactions (LPHI), Université de Montpellier, CNRS UMR 5235, Place Eugène Bataillon, CC107, F-34095 Montpellier cedex 5, France
Tel: +33 467 144 726
E-mail: anne.blanc-potard@umontpellier.frand C. Lionne, Centre de Biologie Structurale (CBS), Université de Montpellier, CNRS UMR 5048, INSERM U1054, 29 rue de Navacelles, F-34090 Montpellier, France
Tel: +33 467 417 721
E-mail: lionne@cbs.cnrs.fr

(Received 25 May 2022, revised 20 July 2022, accepted 27 July 2022)

doi:10.1111/febs.16604

Multidrug resistance is a major public health problem that requires the urgent development of new antibiotics and therefore the identification of novel bacterial targets. The activity of nicotinamide adenine dinucleotide kinase, NADK, is essential in all bacteria tested so far, including many human pathogens that display antibiotic resistance leading to the failure of current treatments. Inhibiting NADK is therefore a promising and innovative antibacterial strategy since there is currently no drug on the market targeting this enzyme. Through a fragment-based drug design approach, we have recently developed a NAD^+-competitive inhibitor of NADKs, which displayed *in vivo* activity against *Staphylococcus aureus*. Here, we show that this compound, a di-adenosine derivative, is inactive against the NADK enzyme from the Gram-negative bacteria *Pseudomonas aeruginosa* (PaNADK). This lack of activity can be explained by the crystal structure of PaNADK, which was determined in complex with $NADP^+$ in this study. Structural analysis led us to design and synthesize a benzamide adenine dinucleoside analogue, active against PaNADK. This novel compound efficiently inhibited PaNADK enzymatic activity *in vitro* with a K_i of 4.6 μM. Moreover, this compound reduced *P. aeruginosa* infection *in vivo* in a zebrafish model.

Abbreviations
APTS, *p*-toluene sulfonic acid; CFU, colony-forming unit; DCM, dichloromethane; DMF, *N,N*-dimethylformamide; DMSO, dimethylsulfoxide; G6PDH, glucose-6-phosphate dehydrogenase; HPLC, high- performance liquid chromatography; HRMS, high-resolution mass spectra; IPTG, isopropyl β-D-1-thiogalactopyranoside; k_{ss}, steady- state rate constant; LB, Luria broth; LmNADK, NADK 1 from *Listeria* monocytogenes; NAD^+, nicotinamide adenine dinucleotide; NADK, NAD kinase; $NADP^+$, nicotinamide adenine dinucleotide phosphate; OD, optical density; PaNADK, NADK from *Pseudomonas* aeruginosa; PBS, Phosphate Bbuffered Ssaline; RMSD, root-mean-square deviation; ROS, reactive oxygen species; R_t, retention time; SaNADK, NADK from *Staphylococcus* aureus; SEC, size exclusion chromatography; TEAA, triethylammonium acetate; TFA, trifluoroacetic acid; THF, tetrahydrofuran; TLC, thin-layer chromatography; TMSOK, potassium trimethylsilanolate; WHO, World Health Organization.

Introduction

Pseudomonas aeruginosa is an environmental Gram-negative bacterium and an opportunistic human pathogen that can cause serious acute infections. It is also responsible for chronic infections in patients with cystic fibrosis, being a major cause of mortality. Indeed, the infection maintains the inflammation, worsening the state of health of infected patients. Due to the increased resistance of bacteria to antibiotics, the World Health Organization (WHO) has listed pathogenic bacteria for which new antibiotics or alternative therapeutic strategies are urgently needed and *P. aeruginosa* is in the priority 1 list defined as critical [1].

Bacterial nicotinamide adenine dinucleotide kinase (NADK, EC2.7.1.23) has been identified as a promising target for the development of new antibiotics [2], NADK being the sole enzyme that phosphorylates nicotinamide adenine dinucleotide (NAD^+) to $NADP^+$. $NADP^+$ is an essential coenzyme converted by different redundant enzymes into NADPH, to provide reducing power in many processes such as oxidative stress response, fatty acid and nucleotide biosynthesis [3,4]. NADK is therefore an essential enzyme for rapidly dividing cells, which need both high macromolecular turnover and an efficient response to oxidative stress, and therefore require high level of NADPH [5]. This is particularly important for bacteria in the context of antibiotic treatment. In fact, three main classes of antibiotics (quinolones, beta-lactams and aminoglycosides) stimulate the production of reactive oxygen species (ROS), which can participate in bacterial cell death [6]. In addition, inactivation of the gene encoding NADK is fatal for all bacteria tested so far [7–12].

By a structural approach, we have shown the originality of the enzymatic mechanism of NADK and of its NAD^+ binding mode [13]. Based on the analysis of the structure of the NADK 1 from *Listeria monocytogenes* (LmNADK), we developed a new class of antibacterial compounds that specifically mimics the particular conformation that NAD^+ adopts in the NADK binding site [14]. This led us to synthesize original compounds targeting bacterial NADKs [2,15]. Optimization of a propargyl-linked di-adenosine led to NKI1 (Fig. 1), a new lead compound active against the Gram-positive bacterium *Staphylococcus aureus* both *in vitro* and *in vivo* in a mouse animal model of infection [16].

Here, we demonstrate the lack of effect of NKI1 *in vitro* on the enzymatic activity of *P. aeruginosa* NADK (PaNADK). We provide an explanation for the absence of PaNADK inhibition by NKI1 based on the crystallographic structure of the enzyme complexed with $NADP^+$ and propose to replace one adenine of NKI1 with a benzamide. This leads to a new molecule, compound **1** (Fig. 1), active *in vitro* on PaNADK enzyme. This new inhibitor is then tested against *P. aeruginosa in vitro* and *in vivo* in zebrafish embryos, which is now an established vertebrate model of infection to validate novel anti-*Pseudomonas* compounds [17,18].

Results

Enzymatic activity of PaNADK is not inhibited by NKI1

The overexpression and purification of the NADK from *P. aeruginosa* was readily obtained using standard protocols (Fig. 2). The enzymatic activity of PaNADK was determined using a coupled system using G6PDH as previously performed for LmNADK [16]. First, we looked for optimal experimental conditions for the *in vitro* activity of PaNADK. The activity of the enzyme was constant over a wide range of pH, from 7 to 10, but was sensitive to the presence of NaCl (Fig. 3). Based on these results, the conditions retained for further *in vitro* measurements of enzyme activity and inhibition were 50 mM Tris pH 7.5, 1 mM $MgCl_2$ and 5 mM DTT.

We determined the values for k_{cat} at 30 °C of 1 s^{-1} and K_m for MgATP of 2 mM. These two parameters are comparable to those determined with other bacterial or eukaryotic cytosolic NADKs [19]. However, in

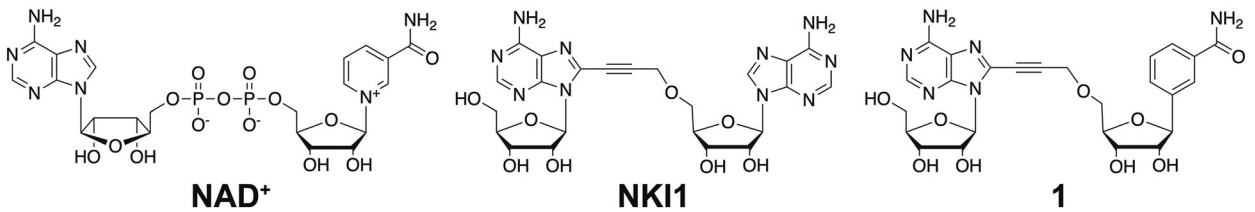

Fig. 1. Chemical structures of compounds used in this study. Structures of NAD^+ (NADK substrate), NKI1 (inhibitor of NADKs from *S. aureus* and *L. monocytogenes*, [16]) and compound **1** (PaNADK inhibitor, this study).

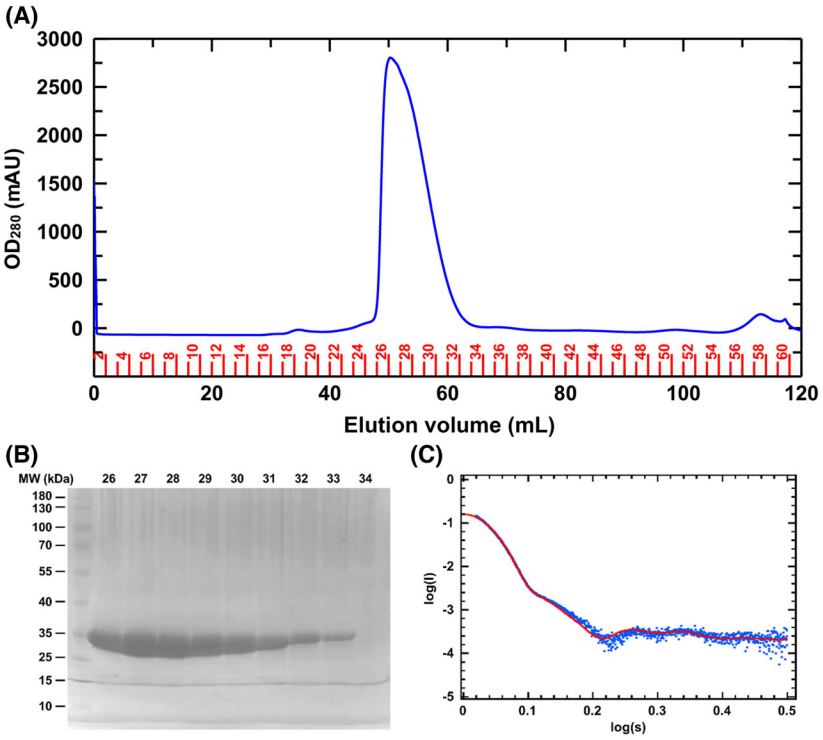

Fig. 2. Purification and biophysical characterization of PaNADK. (A) Elugram from the gel filtration column. OD at 280 nm is shown as blue line. Fraction numbers are shown in red. (B) Verification of the purity of the recombinant PaNADK by SDS/PAGE gel. The numbers of the fractions obtained from the GF are indicated at the top of the gel. (C) Scattering profiles obtained by SAXS on PaNADK and fitting with a tetrameric model. The fitting of homo-tetrameric protein solution scattering obtained from X-ray crystallography (red line) to the experimental scattering obtained from SAXS experiments (blue dots).

contrast to what was described for NADKs from *Bacillus subtilis* [20], *Salmonella typhimurium* [21] or *L. monocytogenes* [13], PaNADK does not display any cooperative activity. Strikingly, the value of K_m determined for NAD^+ with PaNADK (0.15 mM) is clearly lower than the K_m (or $K_{m\ app}$ in the case of cooperative activity) measured with other bacterial NADKs (1–4 mM) from *Escherichia coli* [22], *Salmonella enterica* [5], *Listeria monocytogenes* [13], *Corynebacterium glutamicum* [23] or *Bacillus subtilis* [20]. The highest sensitivity of PaNADK to NAD^+ compared to that of NADKs from other micro-organisms may be related to the relatively low concentration of NAD^+ in *Pseudomonas* [24].

NKI1, whose chemical structure is shown in Fig. 1, was designed based on the crystal structure of the LmNADK [16]. This lead compound was shown to act as a NAD^+ competitive inhibitor of the enzymatic activity of LmNADK with a K_i of 25 μM. NKI1 was also active on the NADK from *Staphylococcus aureus* (SaNADK) with a K_i of 5 μM. Surprisingly, when tested on PaNADK, no significant inhibition was observed up to 50 μM (Fig. 4), suggesting that NKI1 is unable to bind into the active site of PaNADK despite a rather good sequence conservation within the $NADP^+$ binding site and to a lower extent on the whole sequence (Fig. 5).

The crystal structure of PaNADK explains why NKI1 does not inhibit its activity

As for the other bacterial NADKs described so far, PaNADK appeared to be tetrameric in solution from size exclusion chromatography (SEC) analysis (Fig. 2A) and SAXS measurement (Fig. 2C). The SAXS curve showed little trace of structure unfolding and can be nicely fitted with a tetrameric model deduced from homologous structure (e.g. PDB 2AN1) or subsequently from the refined PaNADK structure (see below).

To better understand the lack of effect of NKI1 on PaNADK activity, we determined the atomic structure of the protein bound to $NADP^+$ by X-ray crystallography (Table 1). Crystals were grown in 0.1 M Tris/HCl pH 8.5 and 0.8 M ammonium sulphate and diffracted to 2.3 Å. The structure was solved using molecular replacement and a comparative model extracted from the homologous structure from *Salmonella typhimurium* (PDB 2AN1; 48% of sequence identity). During the course of our study, another structure of PaNADK complexed with $NADP^+$ at a resolution of 2.6 Å was deposited on the PDB (ID 7MH7) without associated publication. It shows no major difference compared with our crystal structure despite a distinct space group. This suggests no major impact from the crystal packing on the two crystal structures.

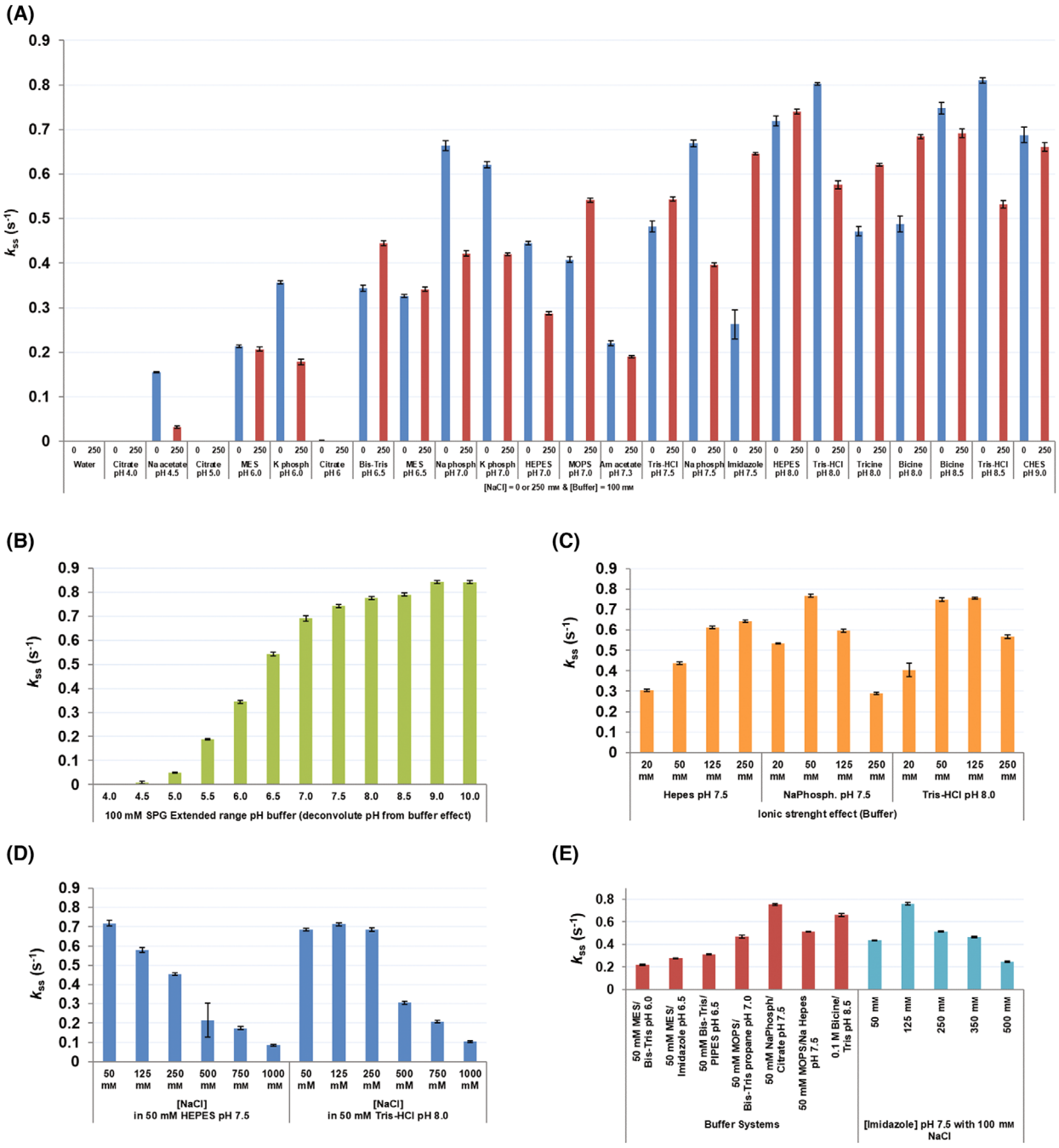

Fig. 3. Screening of optimal *in vitro* experimental conditions for the measurement of PaNADK enzymatic activity. PaNADK activity was measured by an enzyme-coupled system in different conditions using the RUBIC buffer kit. Final concentrations were 1 μM PaNADK, 5 mM MgATP, 5 mM NAD^+, 5 mM glucose-6-phosphate and 1 $U{\cdot}mL^{-1}$ G6PDH. Conditions tested were as follows: (A) buffers (100 mM) of different pHs at low (0 mM NaCl) or high (250 mM NaCl) ionic strength, (B) composite buffer with extended range of pH deconvoluting pH from buffer effect, (C) buffers at different concentrations (20–250 mM), (D) different ionic strengths by variation of NaCl concentration (50–1000 mM) and (E) combination of buffers and effect of imidazole (50–500 mM) in the presence of 100 mM NaCl. Error bars represent calculated standard deviation.

Two monomers were present in the asymmetric unit and highlighted the same fold as the other NADKs. Each monomer is made up of two domains, while the active site is formed at the interface between these two domains where the $NADP^+$ molecule seats. Crystal symmetry allowed to build a tetramer predicted to be

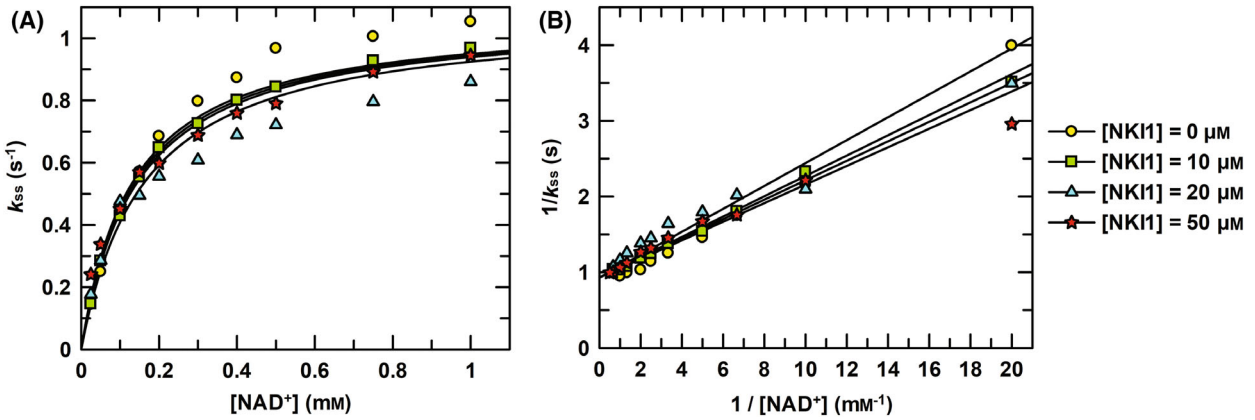

Fig. 4. No significant effect of NKI1 on the enzymatic activity of PaNADK. (A) The steady-state rate constants of PaNADK activity were determined at concentrations of 4 mM of MgATP, 0.05 to 1 mM of NAD^+ and at different concentrations of NKI1, as indicated in the figure. The global fitting of competitive inhibition is shown as lines. (B) Lineweaver–Burk representation of the data showing no significant inhibition of PaNADK by NKI1.

stable in solution according to the size of the buried interface according to PISA [25] and in agreement with our SEC and SAXS data (Fig. 2). The crystal structure of PaNADK is a tetramer consisting of a dimer of dimers (Fig. 6A,B), a conserved organization among all NADKs known so far (except the dimeric human mitochondrial NADK2 described recently [26]). Compared with the structure of the closely related NADK from *S. typhimurium* (which was solved in its apo state and not complexed to $NADP^+$), the overall root-mean-square deviation (RMSD) per monomer and per tetramer is of 1.1 Å (over a common core of 270 residues) and 2.4 Å, respectively. When comparing the structure of PaNADK to the one of LmNADK (PDB 2I2A), which shares only 22% sequence identity, in the same $NADP^+$-liganded state, the RMSD rises to 1.9 Å (243 residues) and 2.5 Å (914 residues) for the monomer and the tetramer, respectively. The PaNADK harbours some specific extensions (Fig. 6C), especially an insertion in the N-terminal domain (residues 37–61) and a distorted C-terminal extension that is partially visible in the electron density (residues 287–294). On the contrary, it lacks the small insertion specific to the Gram-positive bacteria (residues 188–193 in LmNADK). These features of PaNADK sequence are shared by NADKs from other Gram-negative ESKAPE nosocomial pathogens (Fig. 5).

The $NADP^+$ electron density is well defined in our crystal structure (Fig. 6D,E) and provides accurate structural information on the $NADP^+$ binding site of PaNADK. Comparison with the LmNADK-$NADP^+$ complex (PDB ID 2I2A) showed that the sub-site A, which accommodates the adenosine moiety of $NADP^+$, is well conserved while the sub-site N accommodating the nicotinamide ribose moiety showed more variations. In the sub-site A, the main interactions correspond to hydrogen bonds between the adenine moiety and residues N146, T184 and T187 (Fig. 7A) to form the same network as in other known NADKs. As with LmNADK, in the PaNADK sub-site N, $NADP^+$ interacts with the side chains of the conserved D176' (from a second monomer), S192 and D147 residues through hydrogen bonds and with the side chain of Y189 via aromatic stacking (Fig. 7B). The main differences between LmNADK and PaNADK lie in the region of the diphosphate group and the sub-site N. In PaNADK, a two-residue long insertion brings new residues from a second monomer into the active site such as R157′ and M158′. The side chain of R157′ interacts through a salt bridge with one phosphate group of the diphosphate moiety of $NADP^+$ (Fig. 7C). In addition, the following residue, M158′ also interacts with the same phosphate moiety of $NADP^+$ group through a hydrogen bond with its backbone amine while its hydrophobic side chain stacks onto the nicotinamide. Meanwhile, Q247 interacts with the other phosphate of the diphosphate moiety of $NADP^+$. In addition, R94 forms a stabilizing salt bridge with the incoming 2′-phosphate group and K174′ (from a second monomer) forms a hydrogen bond with the 3′ hydroxyl of the phosphorylated ribose, two features not seen before. Of note, R94 appears conserved in NADKs from other Gram-negative bacteria (see alignment). These additional interactions likely explain the higher sensitivity to NAD^+ of PaNADK (K_m = 0.15 mM) than of LmNADK (cooperative kinetics with $S_{0.5}$ = 1.11 mM and Hill coefficient of 1.27 [13]).

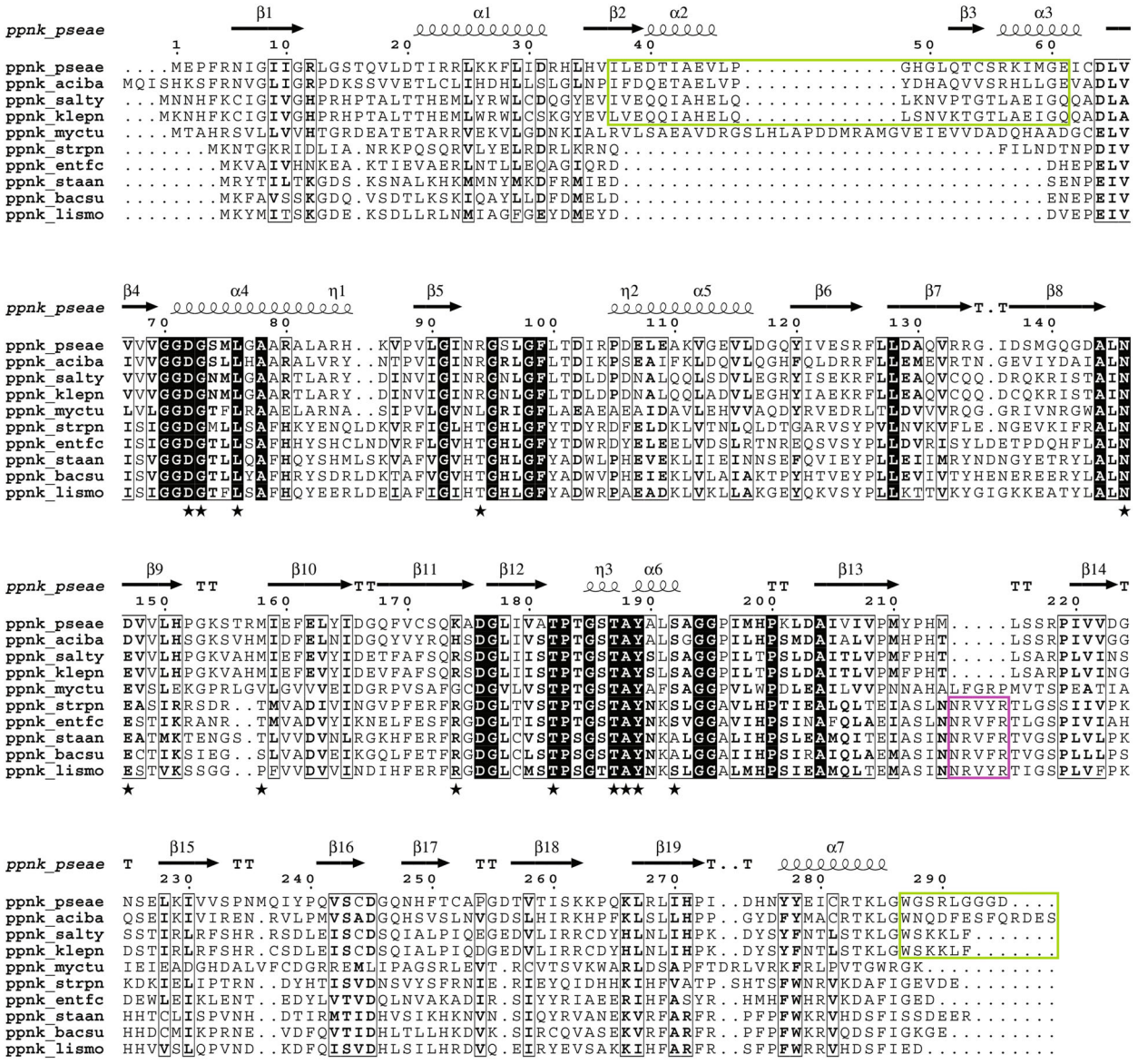

Fig. 5. Sequence alignment of bacterial NADKs. Sequences of bacterial NADKs were aligned and classified from top to bottom as follows: NADKs of Gram-negative bacteria (*Pseudomonas aeruginosa, Acinetobacter baumannii, Salmonella typhimurium* and *Klebsiella pneumoniae*), of *Mycobacterium tuberculosis* and of Gram-positive bacteria (*Streptococcus pneumoniae, Enterococcus faecium, Staphylococcus aureus, Bacillus subtilis* and *Listeria monocytogenes*). Conserved residues are highlighted by black boxes, and conservative substitutions are shown in bold. Extensions specific to Gram-negative and Gram-positive bacteria are highlighted by green and pink boxes, respectively. Residues important for $NADP^+$ binding are indicated by a black star symbol. Secondary structures in PaNADK are shown above the alignment. The figure was drawn using ESPript [44].

The PaNADK structure allowed further comparisons with LmNADK to address NKI1 binding. Although the conformation of $NADP^+$ is identical in both proteins (Fig. 7D), the compound NKI1 does not fit into the PaNADK active site as perfectly as it does in LmNADK. While the adenine moiety replacing the nicotinamide perfectly reproduced the network of hydrogen bonds involving the carbonyl of A185′ and the side chains of S166 and D150′ in LmNADK (Fig. 7E), a 1.1 Å shift in PaNADK leads to two contact losses with the equivalent residues Y211′ and S192 (3.6 and 3.5 Å, respectively), and one important clash with residue D176′ (2.2 Å) (Fig. 7F). These unfavourable interactions may explain the absence of inhibition of

Table 1. Data collection, phasing and refinement statistics for $NADP^+$-bound PaNADK (PDB ID 7QVS).

Ligand	Nicotinamide adenine dinucleotide phosphate ($NADP^+$)
Data collection statistics	
Space group	P 41 2 2
Unit cell dimensions	
a, *b*, *c* (Å)	88.8, 88.8, 174.2
α, β, γ (°)	90.0, 90.0, 90.0
Resolution range (Å)	79.10–2.30 (2.34–2.30)[a]
R_{merge}	0.069 (0.656)[a]
R_{meas}	0.071 (0.669)[a]
R_{pim}	0.014 (0.131)[a]
$I/\sigma I$	39.2 (5.4)[a]
Completeness (%)	100.0 (99.7)[a]
Avg multiplicity	26.2 (25.3)[a]
CC1/2	1.00 (0.96)[a]
Total no. of reflections	832 502 (39 222)[a]
No. of unique reflections	31 752 (1551)[a]
Refinement statistics	
Resolution (Å)	29.59–2.30
No. reflections	31 706
R_{work}/R_{free} (%)	19.7/23.6
No. atoms	
Protein	4284 (Chain A, Chain B)
Ligands	144
Water	231
B-wilson/*B*-average	31.5/41
R.m.s. deviations	
Bond lengths (Å)	0.01
Bond angles (°)	1.52
Ramachandran statistics	
Preferred region (%)	97.00
Allowed region (%)	2.83
Outliers (%)	0.18
Experimental conditions	
Wavelength (Å)	1.00
Temperature (K)	100
Beamline	SLS, X06DA, PXIII
Date and time of collection	18 November 2019, 03:25:15

These statistics are for all measurements used during scale determination—this corresponds to the traditional isotropic analysis.
[a]Values in parentheses are for the highest-resolution shell. Note that data collection and refinement statistics have different highest-resolution shells.

PaNADK by NKI1 and led us to propose a new derivative of NKI1 to fit better the active site of PaNADK.

Structure-based design and synthesis of a new potential inhibitor of PaNADK

Considering the differences in the structure of the PaNADK binding site compared to that of LmNADK, an analogue of NKI1 with a benzamide in place of the adenine in the N sub-site (hereinafter called **1**) was synthesized. Because benzamide is an isosteric analogue of nicotinamide, it was already used for the design of inhibitors targeting NAD^+-utilizing enzymes, in particular IMP dehydrogenase and NADK [27–31]. It should adapt better than adenosine to the nicotinamide binding sub-site of PaNADK.

The synthesis of compound **1** was achieved via a Sonogashira cross-coupling reaction between the 8-bromoadenosine derivative **2** and the benzamide riboside derivative **3** bearing a terminal alkyne functional group at the 5′-position (Scheme 1).

The synthesis of the required alkyne **3** is depicted in Scheme 2. The intermediate benzonitrile **6** was obtained using previously reported procedures with slight modifications [27,30]. Thus, Grignard reaction of commercially available 3-bromobenzonitrile with the ribonolactone **4**, followed by triethylsilane reduction of the anomeric hydroxyl group provided the C-riboside **6** in 73% overall yield.

Next, following route A, conversion of the cyano group into carboxamide **7** by potassium trimethylsilanolate reaction, followed by benzyl ether cleavage using boron tribromide, afforded the benzamide riboside **8** in high overall yield [30]. After protection of the secondary hydroxyl groups as isopropylidene ether, the alkyne was introduced by reaction of **9** with propargyl bromide in the presence of sodium hydride in DMF affording **3** in moderate yield, along with propargylation of carboxamide group. Alternative route B involved debenzylation of **6** into benzonitrile riboside **10**, followed by 2′,3′-hydroxyl protection and 5′-*O*-propargylation into **12** in 87% over two steps. Next, conversion of the cyano group into the carboxyamide derivative **3** was achieved by treatment of **12** with hydrogen peroxide under basic conditions.

Finally, Sonogashira cross-coupling reaction between bromide **2** and alkyne **3**, followed by two-step deprotection of the resulting coupling product **13** afforded the target dinucleotide **1** in 20% overall yield.

Compound 1 inhibits the enzymatic activity of PaNADK and is not cytotoxic

The effect of compound **1** on the enzymatic activity of PaNADK was tested in the same experimental conditions as the ones used for NKI1. Compound **1** was found to be a NAD^+-competitive inhibitor of PaNADK with a K_i value of 4.6 ± 0.3 μM, as shown in Fig. 8.

Given its inhibitory effect on PaNADK enzymatic activity, compound **1** appears as a suitable molecule that may be active against the bacterium

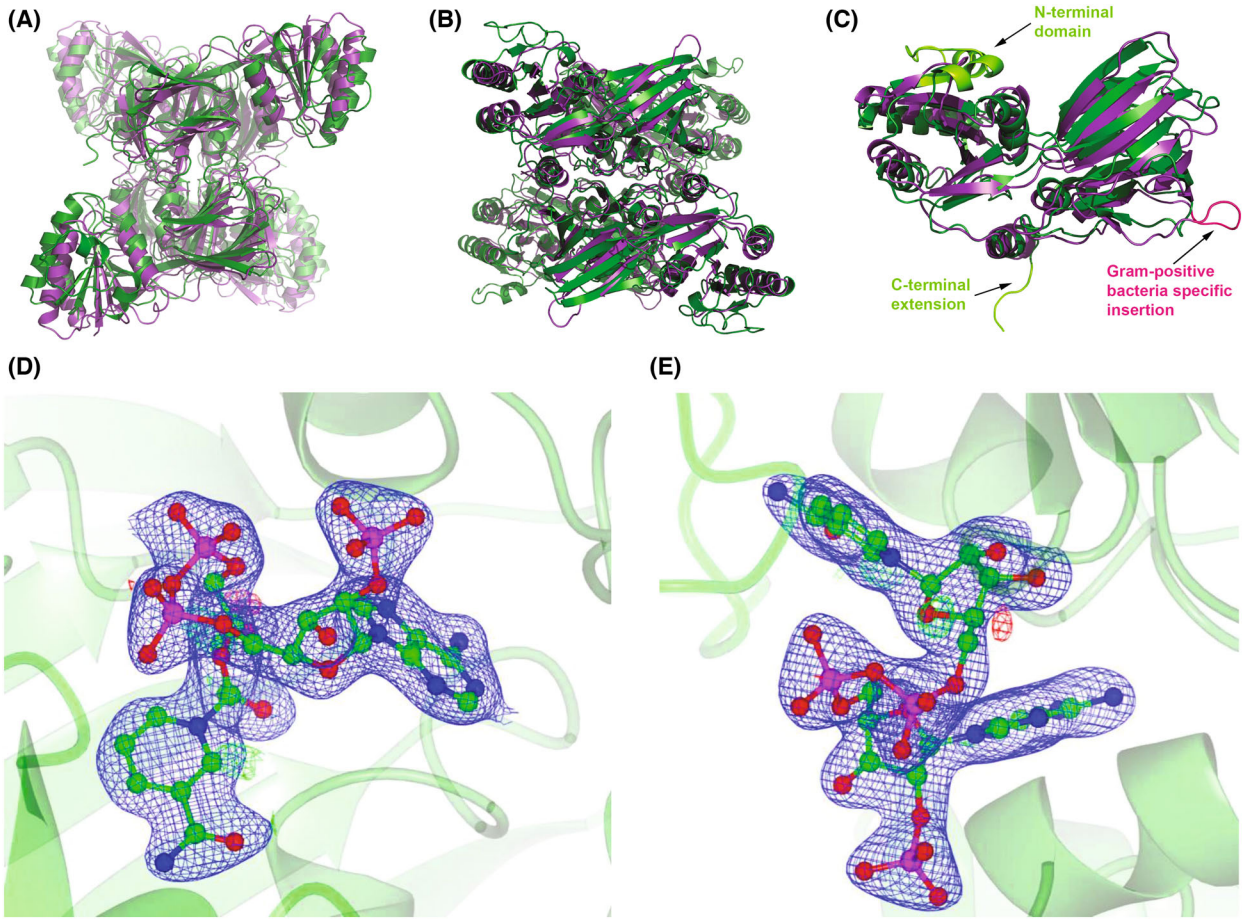

Fig. 6. Comparison of the structure of PaNADK and LmNADK. In all panels, PaNADK and LmNADK structures are shown in green and purple, respectively. (A, B) Superimposed tetrameric form of PaNADK (PDB ID 7QVS) and LmNADK (PDB ID 2I2A) in two different orientations. (C) Superimposed monomeric form of PaNADK and LmNADK highlighting the main structural differences between the two structures, corresponding to extensions or insertions indicated on the sequence alignment (Fig. 5). (D, E) Electron density corresponding to the $NADP^+$ bound to PaNADK. The $2F_o - F_c$ omit map (blue) at a sigma level of 3 is shown in two different orientations. Images of the structures were generated using PYMOL version 2.5.2, Molecular Graphics System, Schrödinger, LLC. The electron density was generated using CCP4MG-2.10.11 software.

P. aeruginosa. Before testing the anti-infectious properties of compound **1**, we have first evaluated its cytotoxicity on human cells using a standard protocol. No cytotoxicity was observed up to concentrations of 50 μM of compound **1** (data not shown), supporting the relevance of further *in vivo* experimentations.

Compound 1 has no effect on *P. aeruginosa* growth *in vitro* but displays an antivirulence effect *in vivo*

The effect of compound **1** was first tested on *P. aeruginosa* growth in liquid cultures. We used PAO1 strain, which is the most commonly *P. aeruginosa* used strain for research. Various concentrations of compound **1** (ranging from 2 to 200 μM, dissolved in 0.01–1% DMSO) were tested, and the corresponding concentrations of DMSO were used as control. No difference in growth curves was found between compound **1**-treated bacteria and DMSO-treated bacteria (Fig. 9). Hence, compound **1** does not affect *P. aeruginosa* growth in these experimental conditions. The lack of antibacterial action in liquid cultures may be linked to conditions (LB medium) that allow growth on a suboptimal pool of NADP(H) and/or to a poor penetration of compound **1** through the bacterial envelope.

We then evaluated the effect of compound **1** *in vivo* in the zebrafish embryo infection model. Zebrafish (*Danio rerio*) is a vertebrate that offers several advantages, in terms of methodological, financial and ethical

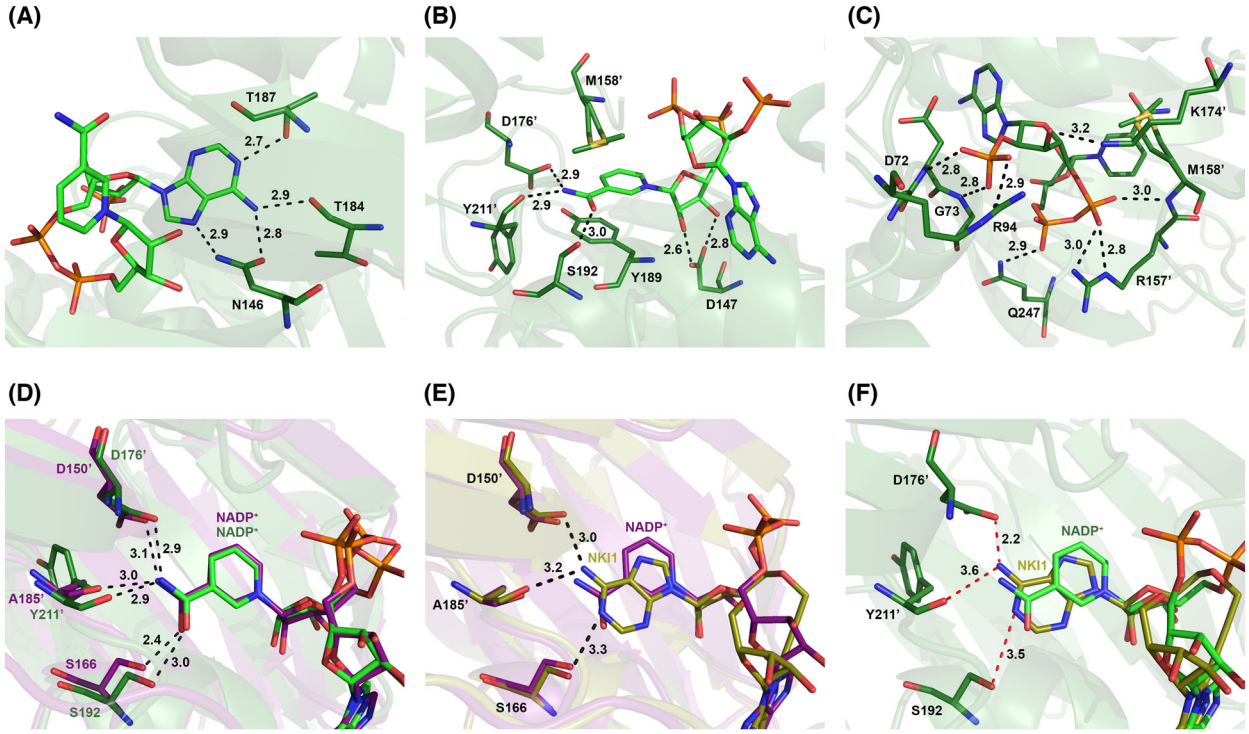

Fig. 7. Detailed analysis of ligand binding sites of PaNADK and LmNADK. In all panels, PaNADK-NADP$^+$ and LmNADK-NADP$^+$ structures are shown in green and purple, respectively. PaNADK interactions with the different groups of NADP$^+$: (A) adenine, (B) nicotinamide ribose and (C) diphosphate and phosphorylated ribose. (D) Comparison of the NADP$^+$ binding sites of PaNADK and LmNADK showing a similar position of the ligand. (E) Superimposition of the structure of the LmNADK-NADP$^+$ (PDB ID 2I2A, in purple) and LmNADK-NKI1 (PDB ID 6RG9, in gold) structure showing favourable interactions with both ligands. (F) Superimposition of the structure of the PaNADK-NADP$^+$ structure (PDB ID 7QVS, green) and PaNADK-NKI1 model (in gold) showing unfavourable interactions with the adenine of NKI1. Images of the structures were generated using PYMOL version 2.5.2, Molecular Graphics System, Schrödinger, LLC.

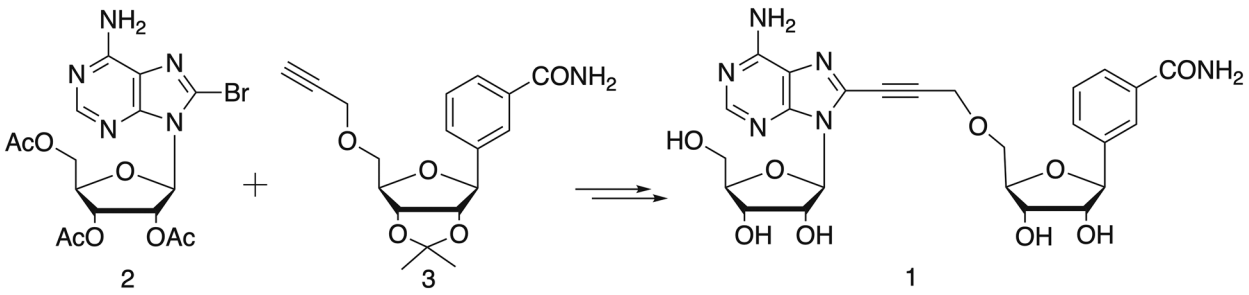

Scheme 1. Synthesis of NAD$^+$ analogue **1** via Sonogashira reaction between bromide **2** and alkyne **3**.

issues, over mammalians models. This model is suitable for *in vivo* chemical screening [32,33] and drug toxicity assays [34], with the advantage that permeability of the larvae allows the entry of small compounds by balneation exposure. Zebrafish embryo has been used with various bacterial pathogens, including *P. aeruginosa* [18,35], and we have recently developed a novel mode of infection, based on bath immersion of injured embryos, to screen anti-infectious compounds efficient against *P. aeruginosa* [17].

We have thus used this bath immersion infection mode with tail-injured zebrafish embryos to address the effect of compound **1** on *P. aeruginosa* virulence. The effect of compound **1**, dissolved in DMSO, was tested at various concentrations on injured embryos immersed with bacterial inoculum at approximately

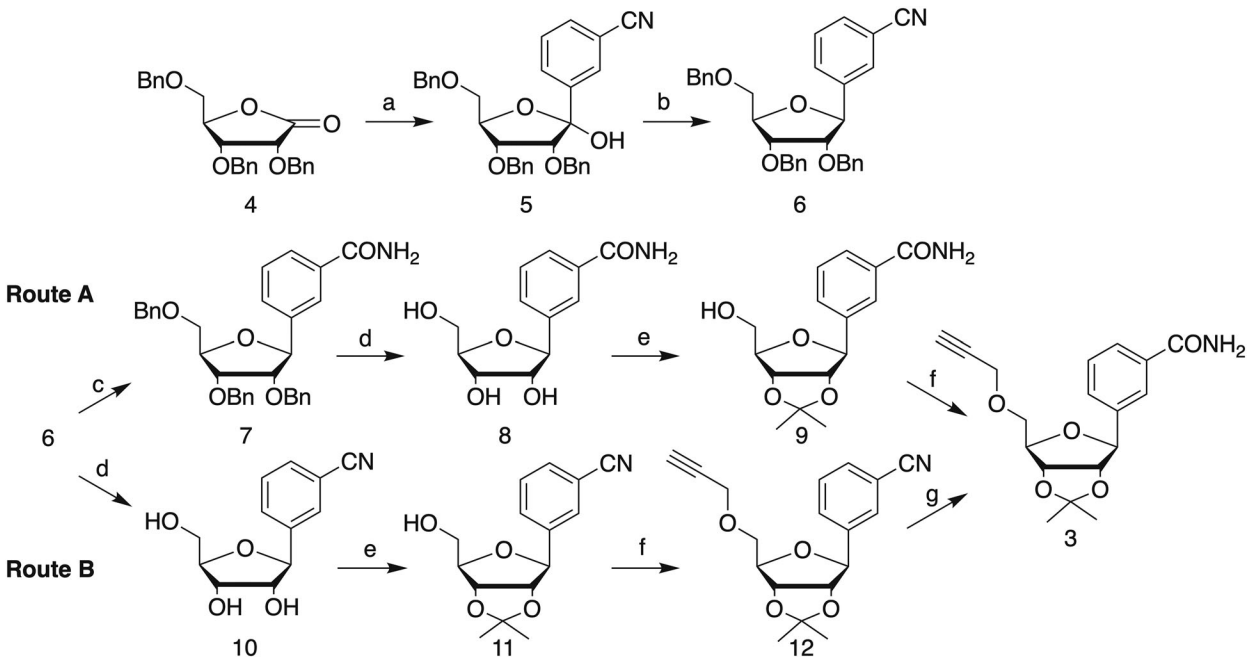

Scheme 2. Synthesis of required alkyne **3**. Reagents and conditions: (a) 5-bromobenzonitrile, n-BuLi, THF, −78 °C; MeOH – 78 °C to rt; (b) BF_3–OEt_2, Et_3SiH, −0 °C to rt; (c) TMSOK, THF, reflux; (d) 1 M BBr_3 in DCM, −78 °C to rt; (e) APTS, acetone, 2,2-dimethoxypropane; (f) propargyl bromide, NaH, DMF, −0 °C; (g) H_2O_2, K_2CO_3, DMSO.

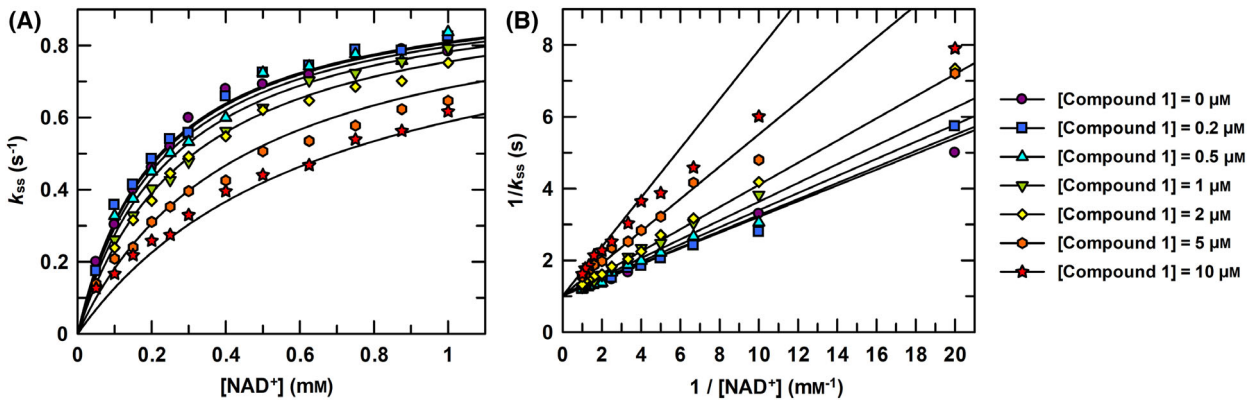

Fig. 8. Inhibition of the enzymatic activity of PaNADK by compound **1**. (A) The steady-state rate constants of PaNADK activity were determined at 4 mM MgATP, 0.05–1 mM NAD^+ and at different concentrations of **1**, as indicated in the figure. Global competitive inhibition fittings are shown as lines. (B) Lineweaver–Burk representation of the data showing a significant competitive inhibition of PaNADK by compound **1**.

8.10^7 CFU·mL^{-1}. Compound **1** was added simultaneously with the bacterial cells following a protocol previously described [17]. In non-treated embryos immersed with PAO1, DMSO was added to reflect the amount of DMSO in compound **1**-treated embryos. Compound **1** at 20 µM exhibited a protective effect since a significant reduction in embryo mortality was observed comparatively to DMSO-treated embryos (Fig. 10A). Importantly, the addition of 20 µM compound **1** was not associated with toxicity for embryos, as shown by the lack of significant mortality upon addition of the sole molecule (Fig. 10B).

Thus, our *in vivo* results indicate an anti-infective potential of this novel compound **1**, without exhibiting any toxicity. Because compound **1** does not display antibacterial activity *in vitro* in the conditions tested, the *in vivo* effect can be qualified as antivirulence effect.

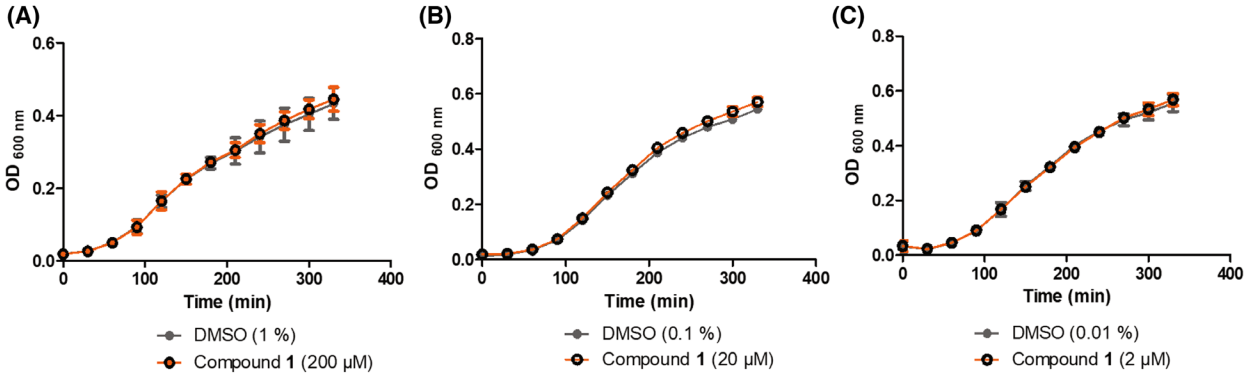

Fig. 9. Effect of compound **1** on *P. aeruginosa* growth in liquid medium. *P. aeruginosa* growth curves in LB medium in the presence of compound **1** at (A) 200, (B) 20 and (C) 2 µM (in 1%, 0.1% or 0.01% DMSO, respectively) or in the presence of the indicated percentage of DMSO as control. Graphs represent the mean of three independent experiments. Error bars represent standard errors of the mean.

Discussion

Inhibiting bacterial NADK is a promising and innovative antimicrobial strategy. A NAD^+-competitive inhibitor, NKI1, which is active against NADK from Gram-positive bacteria, appeared inactive against PaNADK. The structure of PaNADK suggested that, unlike LmNADK, the sub-site N of PaNADK cannot accommodate a ligand such as NKI1, which has an adenine in place of the nicotinamide of NAD^+. In agreement, a novel analogue of NKI1 harbouring a benzamide instead of the clashing adenine (compound **1**) had an inhibition constant value on PaNADK that is comparable to that of NKI1 on LmNADK and SaNADK [16]. NAD^+ analogues with a benzamide moiety in place of the nicotinamide have been previously reported [30], but the most potent competitive inhibitor exhibited only a moderate activity on NADK from *Mycobacterium tuberculosis* (37% inhibition at 2 mM). In the case of compound **1**, the introduction of a propargyl-link contributes to its strong inhibitory activity on purified enzyme, probably due to an increased rigidity of the molecule and a better mimic of the NAD^+ conformation in its binding site.

Compound **1** displays an antivirulence effect *in vivo* in *P. aeruginosa*-infected zebrafish model, without displaying antibacterial activity *in vitro* under the conditions used in this study. Further studies will be required to better understand the mechanism by which compound **1** increases the defensive ability of zebrafish embryos against *P. aeruginosa*. Compound **1** may have an effect on *P. aeruginosa* specifically during infection due to the stressing conditions encountered within the host, such as reactive oxygen species. In addition, or alternatively, we cannot exclude that compound **1** may have other targets than PaNADK *in vivo*.

To a better understanding of its mechanism of action *in vivo*, optimization of compound **1** should be done in the future and its synergy with other antibacterial compounds should be investigated. Compound **1** could also serve as a basis to develop fluorescent or clickable probes that could be used as molecular tools to detect or modulate the activity of NAD^+-dependent enzymes or identify putative alternative targets [36–38]. Importantly, NADKs from Gram-negative bacteria from the ESKAPE group are closely related to PaNADK, suggesting that compound **1** might have an inhibitory effect on the enzymes from other bacterial pathogens as well. According to the World Health Organization, the most critical group of bacteria for which new antibiotics are urgently needed includes multi-resistant *Acinetobacter*, *Pseudomonas* and various *Enterobacteriaceae* such as *Klebsiella*, *E. coli*, *Serratia* and *Proteus* that can cause severe and often deadly infections. In addition, we do not exclude an efficacy of compound **1** against Gram-positive bacteria since it is active on LmNADK with a K_i of 3.2 ± 0.4 µM (data not shown).

In conclusion, we have designed a new inhibitor of bacterial NADK, which is a still orphan therapeutic target. Efficient NADK inhibitors could have a broad activity spectrum and therefore an important impact on the treatment of multiple infectious diseases, including those triggered by these multidrug-resistant and critical bacteria.

Materials and methods

Molecular cloning of the PaNADK gene

A synthetic gene encoding PaNADK (corresponding to *ppnK* gene in PAO1) was optimized for expression in

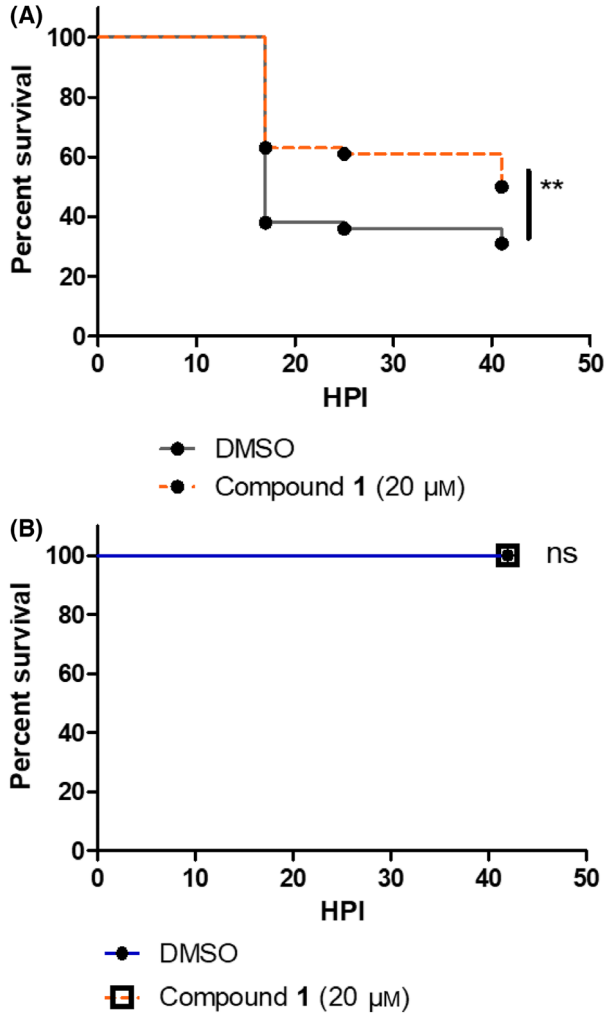

Fig. 10. Evaluation of compound **1** on *Pseudomonas* virulence *in vivo*. (A) The efficacy of compound **1** against *P. aeruginosa* was tested with embryos injured in the tail fin and bath infected with PAO1 suspension at approximately 8.10^7 CFU·mL^{-1} in the presence of compound **1** at 20 µM (in 0.1% DMSO). Injured embryos in the control group were treated with PAO1 suspension in the presence of DMSO at 0.1%. A significant difference ($P < 0.01$) is found in the survival curve of treated versus non-treated embryos. (B) The toxicity of compound **1** at 20 µM was monitored after immersion of embryos injured in the tail fin. For all experiments, the embryo survival was monitored for 45 h and survival curves were represented with a Kaplan–Meier representation. Graphs represent the pool of three minimum independent experiments (n = 120 larvae for compound **1** test or 60 larvae for toxicity test, in total per condition). ** means P value <0.01, ns means no significant difference.

E. coli and ordered from Integrated DNA Technologies, BVBA (Leuven, Belgium). It was amplified with forward primer 5′-CCCTTTCATATGATGGAGCCCTTCCGCA AT-3′ and reverse primer 5′-CCCAAACTCGAGGTCA CCCCCTCCTAAACG-3′ including cleavage sites of restriction enzymes for cloning into pET-22b(+) vector (Q5 Hot Start High-Fidelity 2× Master Mix). The PCR product was then digested using the NdeI and Xho1 restriction enzymes, purified (NucleoSpin Gel and PCR clean-up kit, Macherey-Nagel, Hoerdt, France), and ligated (T4 ligase) into linearized pET-22b(+) vector at the same restriction sites. At the C terminus, the construct codes for two additional amino acids (LE) followed by a 6His-tag. The gene sequence of PaNADK was checked by sequencing (Genewiz, Paris, France).

PaNADK expression and purification

PaNADK protein was overexpressed in *E. coli* BL21 (*DE3*) cells in 2-YT broth with 100 µg·mL^{-1} ampicillin. The protein expression was induced at OD_{600} of 0.7–0.8 with 1 mM isopropyl β-D-1-thiogalactopyranoside (IPTG) overnight at 25 °C. The harvested cells were re-suspended in buffer A (50 mM sodium phosphate pH 8.3, 150 mM NaCl, 10 mM imidazole, 2 mM DTT) supplemented with 1 tablet of cOmplete™ EDTA-free protease inhibitor cocktail (Roche), 5 µg·mL^{-1} of lysozyme (Euromedex), 5 µg·mL^{-1} of DNase (Sigma Aldrich). Bacterial cell disruption was achieved by sonication at 40% amplitude during 5 min (5 s on, 5 s off) with a 6 mm probe on ice. Cellular debris were removed by centrifugation at 20 000 ***g*** for 30 min and followed by filtration through 0.45-µm syringe filter. The bacteria lysate was loaded onto a HisTrap FF column equilibrated with buffer A using Äkta Pure system (GE Healthcare) at 4 °C. The column was washed with buffer A during 15 column volumes to remove unspecific binding proteins, followed by elution using buffer B (50 mM sodium phosphate pH 8.3, 150 mM NaCl, 500 mM imidazole, 2 mM DTT) with a linear gradient of imidazole from 10 to 500 mM in 20 column volumes. The fractions containing the protein were pooled and concentrated using Amicon Ultra 15 centrifugal filters (3 kDa, Merck Millipore) at 4 °C. The concentrated protein was loaded onto a 16/60 Superdex 200 pre-equilibrated with buffer C (50 mM NaH_2PO_4/Na_2HPO_4 pH 8.3, 100 mM NaCl, 5 mM DTT). Finally, the protein was concentrated till 30 mg·mL^{-1}, aliquoted, flash-frozen in liquid nitrogen and stored at −80 °C.

The sequence of the recombinant protein is shown below and corresponds to the sequence of *P. aeruginosa* PAO1 NADK (UniProtKB Q9HZC0) with a LEHHHHHH tag at the C terminus:

MEPFRNIGIIGRLGSTQVLDTIRRLKKFLIDRHLHV
ILEDTIAEVLPGHGLQTCSRKIMGEICDLVVVVGGD
GSMLGAARALARHKVPVLGINRGSLGFLTDIRPDE
LEAKVGEVLDGQYIVESRFLLDAQVRRGIDSMGQ
GDALNDVVLHPGKSTRMIEFELYIDGQFVCSQKA
DGLIVATPTGSTAYALSAGGPIMHPKLDAIVIVPMY
PHMLSSRPIVVDGNSELKIVVSPNMQIYPQVSCDGQ
NHFTCAPGDTVTISKKPQKLRLIHPIDHNYYEICRT
KLGWGSRLGGGDLEHHHHHH.

The expression, solubility and purity of PaNADK were tested on SDS/PAGE gel (Invitrogen™ NuPAGE™ 4–12% gel). The molar absorption coefficient and the absorbance value for 0.1% of the 6His-tagged protein, hereafter named PaNADK, were estimated with the ABIM software (http://bioserv.cbs.cnrs.fr/ABIM/w3bb/d_abim/) at 14 650 M^{-1} cm^{-1} and 0.441 $(g{\cdot}L^{-1})^{-1}{\cdot}cm^{-1}$, respectively.

SAXS

Scattering curves were recorded at the SWING beamline of SOLEIL (Paris-Saclay, France) at X-ray wavelength of 1 Å with the EIGER-4M detector positioned 2 m from the sample using 12 keV X-ray flux. The resulting range of the scattering vector was $0.038 < q < 6.3$ nm^{-1}. The protein samples dialysed against 50 mM Tris/HCl pH 8, 100 mM NaCl, 5 mM DTT buffer during 3 h at 4 °C and centrifuged at 12 000 ***g*** before measurements. Batch measurements were recorded at room temperature over 38 exposures and carefully averaged. To eliminate the contribution of the mobile phase, buffer scattering was collected before and after each sample measurement and subtracted from sample scattering. A dilution series consisting of three protein concentrations (9, 3 and 1 $mg{\cdot}mL^{-1}$) was recorded. Additionally, the scattering curves were recorded in the presence of 2 mM NAD^+ or 2 mM $NADP^+$. Guinier analysis, distance distribution functions P(r) and Kratky analysis of the scattering curves were performed using the ATSAS suite [39]. Crysol was used to fit experimental SAXS data to the protein structure obtained from x-ray crystallography. The goodness of fit obtained from the dimer and its assembly as a tetramer (calculated via PISA) were compared [40].

In vitro enzymatic activity measurements and inhibition assays

The optimum pH, buffer and salt concentration for the *in vitro* enzymatic activity of the recombinant PaNADK were screened using the RUBIC Buffer kit (Molecular Dimensions). The enzymatic reaction was followed at 30 °C in a CLARIOstar plate reader (BMG LABTECH) by measuring the absorbance at 340 nm (OD_{340}) using an enzymatic coupled system involving glucose-6-phosphate dehydrogenase (G6PDH). The reaction mixture was made in a half-area 96-well microplate (Greiner Bio-One Clear UV-Star). It consisted of 42 µL of the RUBIC kit buffers, 4 µL of 12.5 µM PaNADK in Buffer C and 4 µL of Mix (12.5 $U{\cdot}mL^{-1}$ G6PDH, 62.5 mM NAD^+, 62.5 mM MgATP, 62.5 mM glucose-6-phosphate) added at time 0. The final protein and ligand concentrations were 1 µM PaNADK, 1 $U{\cdot}mL^{-1}$ G6PDH, 5 mM NAD^+, 5 mM MgATP and 5 mM glucose-6-phosphate. OD_{340} values were converted to concentrations of produced NADH (i.e. NAD^+ consumed) using a molar absorption coefficient for NADH of 6220 $M^{-1}{\cdot}cm^{-1}$. The value of the steady-state rate constant (k_{ss}) corresponds to the initial slope of NAD^+ consumed per second divided by the concentration of PaNADK. The values of k_{cat} and K_m for NAD^+ were determined from the dependence of k_{ss} on the initial concentration of NAD^+ using the Michaelis–Menten equation.

Inhibition assays were performed as described above at 30 °C in a buffer consisting of 50 mM Tris pH 7.5, 1 mM $MgCl_2$ and 5 mM DTT and a final volume of 100 µL. The final concentrations in the reaction mixtures were 25 nM PaNADK, 1 $U{\cdot}mL^{-1}$ G6PDH, 4 mM MgATP, 5 mM glucose-6-phosphate, 0.05–1 mM NAD^+ and various concentrations of inhibitor (see the legends of the figures). Buffer, NAD^+ and inhibitor solutions (total volume 25 µL, concentration 4×) were dispensed into the microplate using an OT-2 lab robot (Opentrons). The 25 µL of mixture containing G6PDH, MgATP and glucose-6-phosphate at a 4× concentration was dispensed using a manual repeating pipette. Finally, the reaction was started at time 0 by adding and mixing 50 µL of PaNADK at a 2× concentration using a multichannel pipette.

The values of the inhibition constants were determined from the raw values of k_{ss} at different concentrations of NAD^+ and inhibitor using a competitive inhibition equation (Eqn 1). A Lineweaver–Burk transformation of the raw values was used to produce an illustrative double-reciprocal plot of the data.

$$k_{ss} = \frac{k_{cat} \times [NAD^+]}{K_m\left(1 + \frac{[Inhibitor]}{K_i}\right) + [NAD^+]} \quad (1)$$

Fits and graphical representations were made using GraFit software (version 7.0.3, Erithacus Software Ltd).

Crystallization and structure refinement

The protein solution at 10 $mg{\cdot}mL^{-1}$ in 50 mM NaH_2PO_4/Na_2HPO_4 pH 8.3, 100 mM NaCl and 5 mM DTT was pre-incubated 2 h with 10 mM $NADP^+$ (100 mM $NADP^+$ stock solution in 50 mM Tris, pH 6.5) and cleared using 0.22 µm centrifugal filter by centrifugation at 12 000 g. Subsequently, a crystallization screen was applied using six commercially available kits from Qiagen (PEG 1 & 2, pH-Clear 1 & 2, $AmSO_4$ Suite and Classics) handled by crystallization robot (Mosquito, SPT Labtech). 0.1 µL of PaNADK-$NADP^+$ solution and 0.1 µL of reservoir were mixed to equilibrate against 45 µL reservoir solution using the sitting-drop vapour-diffusion method at 18 °C. Crystals appeared within a week in condition N° 77 of $AmSO_4$ Suite (0.1 mM Tris pH 8.5, 1 M ammonium sulphate). Crystal growth was further manually reproduced and optimized in an EasyXtal 15-well plate (NeXtal) by mixing 1 µL of PaNADK-$NADP^+$ solution with 1 µL of reservoir and equilibrating against 500 µL reservoir solution using the

hanging-drop vapour-diffusion method at 18 °C. Crystals formed in the optimal condition (0.1 mM Tris pH 8.5, 0.8 mM ammonium sulphate) were flash-frozen in liquid nitrogen. X-ray diffraction data were collected in the X06DA (PXIII) macromolecular crystallography beamline at the Swiss Light Source. The structure was solved by molecular replacement (CCP4, PHENIX) using as a search model, a comparative model derived from PDB 2AN1, the NADK from *Salmonella typhimurium* LT2. Global Phasing Limited software packages (Buster and Rhofit) were used for a final step of structure refinement [41]. The statistics of X-ray data processing and structure refinement are summarized in Table 1.

Sequence alignment of bacterial NADKs

The primary sequences of bacterial NADKs were extracted from UniProtKB. UniProt entry IDs were Q9HZC0 for *P. aeruginosa* (ppnk_pseae), A0A059ZQ75 for *Acinetobacter baumannii* (ppnk_aciba), P65774 for *Salmonella typhimurium* (ppnk_salty), A6TCM2 for *Klebsiella pneumoniae* (ppnk_klepn), P9WHV7 for *Mycobacterium tuberculosis* (ppnk_myctu), P9WHV7 for *Streptococcus pneumoniae* (ppnk_strpn), Q3XWF9 for *Enterococcus faecium* (ppnk_entfc), H6UH60 for *Staphylococcus aureus* (ppnk_staau), O31612 for *Bacillus subtilis* (ppnk_bacsu) and Q8Y8D7 for *Listeria monocytogenes* (ppnk_lismo). Sequences were aligned using ViTO software [42].

Chemical synthesis

General

The general methods have already been described in [15]. All commercially available reagents and solvents, unless otherwise stated, were used without purification. Anhydrous reactions were carried out under an argon atmosphere. Analytical thin-layer chromatography (TLC) was performed on TLC plates pre-coated with silica gel 60 F_{254}. Compounds were visualized with UV light (254 nm) and by spraying with a mixture of ethanol/anisaldehyde/sulfuric acid/acetic acid (90/5/4/1), followed by heating. Reactions were also monitored using an HPLC system (Agilent 1100 equipped with a C18 reverse phase column) coupled to a mass spectrometer (ESI source). Flash chromatography was performed with silica gel 60 (230–400 mesh). HPLC purification was carried out on an Agilent system (1100 Series) equipped with a diode array detector using a C18 reverse phase column (Kromasil, 5 µm, 100 Å, 150 × 4.6 mm) and a linear gradient of acetonitrile in 10 mM triethylammonium acetate (TEAA) buffer over 15 or 20 min at a flow rate of 4 mL·min^{-1}. Retention time (R_t) and elution conditions are specified. The purity of tested compounds was at least 96% pure as determined by HPLC. NMR spectra (Appendix S1) were recorded on Bruker Avance 400 (^{1}H at 400.13 MHz and ^{13}C at 100.62 MHz). Chemical shifts (δ) are reported in ppm relative to the solvent signals. Coupling constants (J values) are reported in Hz. The complete assignment of ^{1}H and ^{13}C signals was performed by analysis of the correlated homonuclear {H,H}-COSY and heteronuclear {H,C}-HMBC, {H,C}-HSQC spectra. High-resolution mass spectra (HRMS) were recorded with a Q-Tof Micro mass spectrometer under electrospray ionization in positive ionization mode using a mobile phase of acetonitrile/water with 0.1% formic acid.

NKI1 was prepared as described previously [16].

3-(2,3,5-tri-*O*-benzyl-β-D-ribofuranosyl)benzonitrile (6)

The title compound was prepared following reported procedures with slight modifications [27,30]. To a solution of 3-bromobenzonitrile (3.81 g, 21 mmol) in dry tetrahydrofuran (THF) (72 mL) containing activated 4 Å molecular sieves (5 g) was slowly added n-BuLi (2.5 M in hexane, 9.2 mL) at –78 °C under an argon atmosphere. Stirring was maintained for 20 min after addition was completed, and then a solution of ribonolactone **4** (2.51 g, 6 mmol) in THF (24 mL) was slowly added to the reaction mixture at –78 °C. After 30 min, anhydrous MeOH (7.3 mL) was added at the temperature allowed to warm to room temperature. The reaction mixture was neutralized by adding 2 N HCl (12 mL) and extracted with sat. $NaHCO_3$ (150 mL). The organic phase was dried and concentrated under reduced pressure, and the residue was purified by flash column chromatography (180 g silica gel, 5–15% ethyl acetate in cyclohexane) affording hemiacetal **5** (2.77 g, 88.5%). To a solution of **5** (2.75 g, 5.3 mmol) in dry dichloromethane (DCM) (26.5 mL) at 0 °C was added Et_3SiH (3.37 mL, 21.1 mmol). After stirring for 5 min, $BF_3{\cdot}Et_2O$ (1.31 mL, 10.6 mmol) was slowly added and the resulting mixture was warmed to room temperature over 10 min. Then, E_3N (7.39 mL, 53 mmol) was added, and the reaction mixture was concentrated under reduced pressure. The residue was purified by flash column chromatography (5–10% ethyl acetate in cyclohexane) to give **6** (2.23 g, 83.2%). ^{1}H NMR (400 MHz, DMSO-d_6): δ 3.64 (dd, J = 3.9 Hz, J = 10.6 Hz, 1H, H-5′), 3.71 (dd, J = 3.7 Hz, J = 10.6 Hz, 1H, H-5″), 3.93 (dd, J = 5.2 Hz, J = 6.4 Hz, 1H, H-2′), 4.11 (t, J = 4.4 Hz, 1H, H-3′), 4.29 (q, J = 3.6 Hz, 1H, H-4′), 4.44–4.61 (m, 6 H, CH_2 Bn), 4.95 (d, J = 6.6 Hz, 1H, H-1′), 7.18–7.40 (m, 15 H, H Bn), 7.50 (t, 1H, H Ph), 7.71 (d, 1H, H Ph), 7.75 (d, 1H, H Ph), 7.78 (s, 1H, H Ph); ^{13}C NMR (100 MHz, DMSO-d_6): δ 70.64 (C-5′), 71.55, 71.71 and 72.95 (CH_2 Bn), 77.72 (C-3′), 81.28 (C-1′), 82.03 (C-4′), 83.85 (C-2′), 111.74 and 119.18 (Cq), 127.87, 127.93, 128.02, 128.09, 128.29, 128.59, 128.67, 128.75, 129.86, 130.10, 131.63 and 131.89 (CH Ph), 138.37, 138.66 and 142.78 (Cq Ph); HRMS (ESI$^+$-TOF): m/z calcd for $[C_{33}H_{31}NO_4 + H]^+$ 506.2326, found 506.2320.

3-(2,3,5-tri-*O*-benzyl-β-D-ribofuranosyl)benzamide (7)

To compound **6** (2.22 g, 4.4 mmol) in anhydrous THF (11 mL) was added TMSOK (0.845 g, 6.6 mmol) in a sealed tube. After stirring at 70 °C for 24 h, ethanol was added to the reaction mixture, then volatiles were removed under reduced pressure and the residue was purified by flash column chromatography (100 g silica gel, 0–2% MeOH in DCM) affording **7** (1.92 g, 83.5%). ^{1}H NMR (400 MHz, DMSO-d_6): δ 3.60–3.72 (m, 2H, H-5′ and H-5″), 3.94 (dd, J = 5.4 Hz, J = 7.1 Hz, 1H, H-2′), 4.06–4.11 (m, 1H, H-4′), 4.24–4.30 (m, 1H, H-3′), 4.45–4.61 (m, 6H, CH_2 Bn), 4.93 (d, J = 6.8 Hz, 1H, H-1′), 7.19–7.40 (m, 18H, 15H Bn, H Ph and $CONH_2$), 7.55 (d, 1H, H Ph), 7.79 (d, 1H, H Ph), 7.92 (br, 1H, H Ph); ^{13}C NMR (100 MHz, DMSO-d_6): δ 70.82 (C-5′), 71.51, 71.69 and 72.93 (CH_2 Bn), 77.89 (C-3′), 81.79 (C-1′), 82.13 (C-4′), 83.91 (C-2′), 111.74 (Cq), 126.10, 127.17, 127.87, 127.91, 127.93, 128.01, 128.27, 128.51, 128.59, 128.67, 128.73 and 129.44 (CH), 134.83 (Cq Ph), 138.48, 138.71 and 138.96 (Cq Bn), 141.11 (Cq Ph), 168.33 (CO); HRMS (ESI$^+$-TOF): m/z calcd for $[C_{33}H_{33}NO_5 + H]^+$ 524.2431, found 524.2429.

3-(β-D-ribofuranosyl)benzamide (8)

A 1 M solution of BBr_3 in DCM (14.6 mL) was added dropwise to a stirred and cooled to −78 °C solution of **7** (1.91 g, 3.6 mmol) in anhydrous DCM (72 mL) containing molecular sieves. After a 1 h at −78 °C, the mixture was allowed to warm to room temperature and stirred overnight. The reaction was quenched by adding diethyl ether/water (4/1, 180 mL) at 4 °C for 20 min, and then the volatiles were removed under reduced pressure. Purification by flash column chromatography (115 g silica gel, 10 to 12% MeOH in DCM) afforded **8** (0.76 g, 83%). ^{1}H NMR (400 MHz, DMSO-d_6): δ 3.54 (dd, J = 4.8 Hz, J = 11.6 Hz, 1H, H-5′), 3.59 (dd, J = 4.4 Hz, J = 11.6 Hz, 1H, H-5″), 3.71 (dd, J = 5.4 Hz, J = 7.1 Hz, 1H, H-2′), 3.83 (t, J = 4.6 Hz, J = 8.3 Hz, 1H, H-4′), 3.90 (dd, J = 3.6 Hz, J = 5.4 Hz, 1H, H-3′), 4.60 (d, J = 7.1 Hz, 1H, H-1′), 7.32 (br, 1H, $CONH_2$), 7.40 (t, 1H, H Ph), 7.55 (d, 1H, H Ph), 7.77 (d, 1H, H Ph), 7.86 (s, 1H, H Ph), 7.94 (br, 1H, $CONH_2$); ^{13}C NMR (100 MHz, DMSO-d_6): δ 62.51 (C-5′), 71.85 (C-3′), 77.94 (C-2′), 83.33 (C-1′), 85.71 (C-4′), 125.91, 126.84, 128.36 and 129.56 (CH Ph), 134.59 and 141.93 (Cq Ph), 168.46 (CO); HRMS (ESI$^+$-TOF): m/z calculated for $[C_{12}H_{15}NO_5 + H]^+$ 254.1023, found 254.1025.

3-(2,3-*O*-isopropylidene-β-D-ribofuranosyl)benzamide (9)

To a suspension of **8** (0.76 g, 3.0 mmol) in acetone (30 mL) were added 2,2-dimethoxypropane (1.11 mL, 9.0 mmol) and APTS (0.57 g, 3.0 mmol). After stirring overnight at room temperature, the reaction was quenched by the addition of 1 M Na_2CO_3 (15 mL), concentrated under reduced pressure and then extracted twice with ethyl acetate. The organic layers were dried over Na_2SO_4, filtered and concentrated under reduced pressure. Purification by flash column chromatography (40 g silica gel, 5% MeOH in DCM) afforded **9** (0.58 g, 66%). ^{1}H NMR (400 MHz, DMSO-d_6): δ 1.30 (s, 3H, CH_3 isop), 1.55 (s, 3H, CH_3 isop), 3.56 (dd, 1H, H-5′), 3.61 (dd, 1H, H-5″), 4.01 (q, J = 4.7 Hz, J = 8.8 Hz, 1H, H-4′), 4.53 (dd, J = 5.4 Hz, J = 6.7 Hz, 1H, H-2′), 4.69 (dd, J = 3.8 Hz, J = 6.7 Hz, 1H, H-3′), 4.79 (d, J = 5.4 Hz, 1H, H-1′), 4.92 (t, 1H, OH), 7.36 (br, 1H, $CONH_2$), 7.44 (t, 1H, H Ph), 7.53 (d, 1H, H Ph), 7.80 (d, 1H, H Ph), 7.85 (s, 1H, H Ph), 7.96 (br, 1H, $CONH_2$); ^{13}C NMR (100 MHz, DMSO-d_6): δ 25.86 (CH_3 isop), 27.86 (CH_3 isop), 61.99 (C-5′), 82.22 (C-3′), 84.99 (C-1′), 85.23 (C-4′), 86.54 (C-2′), 114.34 (Cq isop), 125.70, 127.24, 128.69 and 129.34 (CH Ph), 134.85 and 140.55 (Cq Ph), 168.23 (CO); HRMS (ESI$^+$-TOF): m/z calcd for $[C_{15}H_{19}NO_5 + Na]^+$ 316.1155, found 316.1151.

3-(β-D-ribofuranosyl)benzonitrile (10)

A 1 M solution of BBr_3 in DCM (0.8 mL) was added dropwise to a stirred and cooled to −78 °C solution of **6** (100 mg, 0.2 mmol) in anhydrous DCM (4 mL) containing molecular sieves. After a 1 h at −78 °C, the mixture was allowed to warm to room temperature and stirred overnight. The reaction was quenched by adding diethyl ether/water (4/1, 10 mL) at 4 °C for 20 min, and then the volatiles were removed under reduced pressure. Purification by flash column chromatography (82 g silica gel, 5–8% MeOH in DCM) afforded **10** (37 mg, 79%). ^{1}H NMR (400 MHz, DMSO-d_6): δ 3.54 (dd, J = 4.3 Hz, J = 11.7 Hz, 1H, H-5′), 3.60 (dd, J = 4.0 Hz, J = 11.7 Hz, 1H, H-5″), 3.68 (dd, J = 5.3 Hz, J = 7.4 Hz, 1H, H-2′), 3.84–3.88 (m, 1H, H-4′), 3.93 (dd, J = 3.2 Hz, J = 5.2 Hz, 1H, H-3′), 4.63 (d, J = 7.4 Hz, 1H, H-1′), 7.55 (t, 1H, H Ph), 7.72 (d, 1H, H Ph), 7.74 (d, 1H, H Ph), 7.85 (br, 1H, H Ph); ^{13}C NMR (100 MHz, DMSO-d_6): δ 62.30 (C-5′), 71.88 (C-3′), 78.27 (C-2′), 82.23 (C-1′), 86.06 (C-4′), 111.56 (CN), 119.40 (Cq), 129.73, 129.96, 131.51 and 131.53 (CH Ph), 143.71 (Cq Ph); HRMS (ESI$^+$-TOF): m/z calcd for $[C_{12}H_{13}NO_4\text{-}H]^+$ 234.0772, found 234.0767.

3-(2,3-*O*-isopropylidene-β-D-ribofuranosyl)benzonitrile (11)

To a suspension of **10** (0.30 g, 1.28 mmol) in acetone (13 mL) were added 2,2-dimethoxypropane (0.47 mL, 3.84 mmol) and APTS (0.24 g, 1.28 mmol). After stirring overnight at room temperature, the reaction was quenched by the addition of 1 M Na_2CO_3 (6.5 mL) and volatiles were removed under reduced pressure and then extracted twice with DCM (3 × 50 mL). The organic layers were dried over

Na_2SO_4, filtered and concentrated under reduced pressure. Purification by flash column chromatography (25 g silica gel, 0–1.5% MeOH in DCM) afforded **11** (0.30 g, 86%). ^{1}H NMR (400 MHz, DMSO-d_6): δ 1.30 (s, 3H, CH_3 isop), 1.55 (s, 3H, CH_3 isop), 3.56 (dd, J = 4.7 Hz, J = 5.4 Hz, 2H, H-5′ and H-5″), 4.04 (q, J = 4.4 Hz, 1H, H-4′), 4.50 (dd, J = 5.7 Hz, J = 6.4 Hz, 1H, H-2′), 4.70 (dd, J = 3.6 Hz, J = 6.6 Hz, 1H, H-3′), 4.83 (d, J = 5.4 Hz, 1H, H-1′), 4.96 (t, 1H, OH), 7.58 (t, 1H, H Ph), 7.71 (d, 1H, H Ph), 7.78 (dt, 1H, H Ph), 7.85 (s, 1H, H Ph); ^{13}C NMR (100 MHz, DMSO-d_6): δ 25.87 (CH_3 isop), 27.85 (CH_3 isop), 61.87 (C-5′), 82.12 (C-3′), 84.51 (C-1′), 85.08 (C-4′), 86.51 (C-2′), 111.89 (CN), 114.25 (Cq isop), 119.18 (Cq), 129.97, 130.05, 131.45 and 131.99 (CH Ph), 142.26 (Cq Ph); HRMS (ESI$^+$-TOF): m/z calcd for $[C_{15}H_{17}NO_4 + H]^+$ 276.1230, found 276.1231.

3-(2,3-*O*-isopropylidene-5-*O*-propargyl-β-D-ribofuranosyl)benzonitrile (12)

Sodium hydride (60% in oil, 32 mg, 0.8 mmol) was added to an ice-cooled solution of **11** (55 mg, 0.2 mmol) in DMF (2 mL) containing molecular sieves. After stirring at 0 °C for 2 h, a solution of propargyl bromide (80% in toluene, 45 µL, 0.4 mmol) was added dropwise. After stirring at 0 °C for 1 h, acetic acid (60 µL) was added and the reaction solution was stirred for an additional 1 h. Water (3 mL) was added, and the mixture was extracted with DCM (3 × 30 mL). The organic layers were dried over Na_2SO_4, filtered and concentrated under reduced pressure. Purification by flash column chromatography (10 g silica gel, 0–1% MeOH in DCM) afforded **12** (54 mg, 86%). ^{1}H NMR (400 MHz, DMSO-d_6): δ 1.30 (s, 3H, CH_3 isop), 1.55 (s, 3H, CH_3 isop), 3.45 (t, J = 2.4 Hz, 1H, C ≡ CH), 3.62–3.70 (m, 2H, H-5′ and H-5″), 4.17 (q, J = 4.5 Hz, 1H, H-4′), 4.21 (d, J = 2.4 Hz, 2H, CH_2-C≡), 4.56 (dd, J = 5.2 Hz, J = 6.5 Hz, 1H, H-2′), 4.68 (dd, J = 3.8 Hz, J = 6.6 Hz, 1H, H-3′), 4.87 (d, J = 5.0 Hz, 1H, H-1′), 7.60 (t, 1H, H Ph), 7.51 (d, 1H, H Ph), 7.70 (d, 1H, H Ph), 7.78 (s, 1H, H Ph), 7.79 (d, 1H, H Ph); ^{13}C NMR (100 MHz, DMSO-d_6): δ 25.85 (CH_3 isop), 27.78 (CH_3 isop), 58.41 (***C***H_2-C≡), 69.90 (C-5′), 77.91 (***C*** ≡ CH), 80.42 (C ≡ ***C***H), 82.23 (C-3′), 83.07 (C-4′), 84.68 (C-1′), 86.37 (C-2′), 111.93 (CN), 114.49 (Cq isop), 119.10 (Cq Ph), 129.92, 130.15, 131.39 and 132.08 (CH Ph), 140. 28 (Cq Ph), 141.99 (Cq Ph); HRMS (ESI$^+$-TOF): m/z calcd for $[C_{18}H_{19}NO_4 + H]^+$ 314.1387, found 314.1385.

3-(2,3-*O*-isopropylidene-5-*O*-propargyl-β-D-ribofuranosyl)benzamide (3)

From **9** (route A): Sodium hydride (60% in oil, 84 mg, 2.1 mmol) was added at −10 °C to a solution of **8** (0.21 g, 0.7 mmol) in DMF (21 mL) containing molecular sieves. After stirring at −10 °C for 2 h, a solution of propargyl bromide (80% in toluene, 78 µL, 0.7 mmol) in DMF (1 mL) was added dropwise. After 2 h at −10 °C, acetic acid (210 µL) was added and the reaction solution was stirred for an additional 1 h. Water was added, and the mixture was extracted with DCM (3 times). The organic layers were dried over Na_2SO_4, filtered and concentrated under reduced pressure. Purification by flash column chromatography (25 g silica gel, 0 to 3% MeOH in DCM) afforded **3** (94 mg, 41%).

From **12** (route B): To an ice-cooled solution of **11** (94 mg, 0.3 mmol) in DMSO (5 mL) in the presence of K_2CO_3 (180 mg, 1.3 mmol) was added H_2O_2 (35% wt in H_2O, 0.166 mL, 1.9 mmol). After stirring for 2 h at room temperature, volatiles were removed by lyophilization. Purification by flash column chromatography (12 g silica gel, 3% MeOH in DCM) afforded **3** (69 mg, 70%).

^{1}H NMR (400 MHz, DMSO-d_6): δ 1.31 (s, 3H, CH_3 isop), 1.55 (s, 3H, CH_3 isop), 3.45 (t, J = 2.4 Hz, 1H, C ≡ CH), 3.66 (d, J = 5.0 Hz, 2H, H-5′ and H-5″), 4.14 (dd, J = 5.0 Hz, J = 9.2 Hz, 1H, H-4′), 4.22 (d, J = 2.4 Hz, 2H, CH_2-C≡), 4.57 (dd, J = 5.2 Hz, J = 6.7 Hz, 1H, H-2′), 4.67 (dd, J = 4.0 Hz, J = 6.8 Hz, 1H, H-3′), 4.82 (d, J = 5.2 Hz, 1H, H-1′), 7.36 (br, 1H, $CONH_2$), 7.45 (t, 1H, H Ph), 7.51 (d, 1H, H Ph), 7.83 (d, 1H, H Ph), 7.85 (s, 1H, H Ph), 7.99 (br, 1H, $CONH_2$); ^{13}C NMR (100 MHz, DMSO-d_6): δ 25.85 (CH_3 isop), 27.80 (CH_3 isop), 58.42 (***C***H_2-C≡), 69.93 (C-5′), 77.90 (***C*** ≡ CH), 80.50 (C ≡ ***C***H), 82.25 (C-3′), 85.01 (C-4′), 85.40 (C-1′), 86.46 (C-2′), 114.64 (Cq isop), 125.74, 127.28, 128.76 and 129.24 (CH Ph), 134.90 and 140.28 (Cq Ph), 168.24 (CO); HRMS (ESI$^+$-TOF): m/z calcd for $[C_{18}H_{21}NO_5 + Na]^+$ 354.1312, found 354.1299.

5-*O*-[3-(2′,3′,5′-tri-*O*-acetyl-adenosin-8-yl)prop-2-yn-1-yl]-1-deoxy-1-(3-carbamoylphenyl)-2,3-*O*-isopropylidene-β-D-ribofuranose (13)

To an argon-purged flask containing bromide **2** (284 mg, 0.6 mmol) and alkyne **3** (133 mg, 0.4 mmol) in THF (4 mL) were added under argon atmosphere triethylamine (167 µL, 1.2 mmol), CuI (8 mg, 0.04 mmol) and tetrakis (triphenylphosphine)palladium (23 mg, 0.02 mmol). The reaction mixture was heated at 60 °C for 1 h under argon atmosphere and concentrated under reduced pressure, and the residue was purified by flash column chromatography (40 g SiO_2, 0–5% MeOH in DCM) affording **13** (145 mg, 50%). ^{1}H NMR (400 MHz, DMSO-d_6): δ 1.30 (s, 3H, CH_3 isop), 1.55 (s, 3H, CH_3 isop), 1.94 (s, 3H, CH_3 OAc), 2.05 (s, 3H, CH_3 OAc), 2.10 (s, 3H, CH_3 OAc), 3.80 (d, J = 5.3 Hz, 2H, H-5′b and H-5″b), 4.13–4.22 (m, 2H, H-4′b and H-5′a), 4.32–4.38 (m, 1H, H-4′a), 4.42 (dd, J = 3.5 Hz, J = 12.0 Hz, 1H, H-5″a), 4.59 (dd, J = 5.2 Hz, J = 6.6 Hz, 1H, H-2′b), 4.65 (br, 2H, CH_2-C≡), 4.72 (dd, J = 4.1 Hz, J = 6.8 Hz, 1H, H-3′b), 4.82 (d, J = 5.2 Hz,

1H, H-1′b), 5.73–5.78 (m, 1H, H-3′a), 6.16 (d, J = 4.3 Hz, 1H, H-2′a), 6.21 (dd, J = 4.3 Hz, J = 6.0 Hz, 1H, H-1′a), 7.40 (br, 1H, $CONH_2$), 7.44 (t, J = 7.5 Hz, 1H, H Ph), 7.53 (d, 1H, H Ph), 7.66 (br, 2H, NH_2), 7.82 (dd, J = 6.3 Hz, J = 6.3 Hz, 1H, H Ph), 7.86 (s, 1H, H Ph), 8.02 (br, 1H, $CONH_2$), 8.22 (s, 1H, H-2a); ^{13}C NMR (100 MHz, DMSO-d_6): δ 20.65 (CH_3 OAc), 20.76 (CH_3 OAc), 20.82 (CH_3 OAc), 25.84 (CH_3 isop), 27.79 (CH_3 isop), 58.83 (***C***H_2-C≡), 62.87 (C-5′a), 70.17 (C-3′a), 70.43 (C-5′b), 71.88 (C-2′a), 75.30 (CH_2-***C*** ≡ C), 79.64 (C-4′a), 82.19 (C-3′b), 82.89 (C-4′b), 85.42 (C-1′b), 86.45 (C-2′b), 87.29 (C-1′a), 93.12 (CH_2-C ≡ ***C***), 114.75 (Cq isop), 119.36 (C-5), 125.80, 127.29, 128.78 and 129.22 (CH Ph), 132.73 (C-8), 134.92 and 140.19 (Cq Ph), 149.14 (C-4), 154.56 (C-2), 156.53 (C-6), 168.17 ($CONH_2$), 169.86 (2C, CO Ac), 170.42 (CO Ac); HRMS (ESI$^+$-TOF): m/z calcd for $[C_{34}H_{38}N_6O_{12} + H]^+$ 723.2620, found 723.2618.

5-*O*-[3-(adenosin-8-yl)prop-2-yn-1-yl]-1-deoxy-1-(3-carbamoylphenyl)-β-D-ribofuranose (1)

Compound **13** (133 mg, 0.18 mmol) was treated with 28% aq. ammonia (1 mL) in MeOH (2 mL) at room temperature for 5 h. After removal of the volatiles, the residue was then treated with an ice-cooled solution of 70% aqueous TFA (5 mL) for 4 h, then the volatiles were removed by lyophilization, and the residue was purified by reverse phase HPLC (linear gradient of 15–25% acetonitrile in 10 mM TEAA over 15 min) affording **1** as a white foam (40 mg, 40%). ^{1}H NMR (400 MHz, DMSO-d_6): δ 3.49–3.60 (m, 1H, H-5′a), 3.66–3.84 (m, 4H, H-5″a, H-2′b, H-5′b and H-5″b), 3.87–3.94 (m, 1H, H-3′b), 3.97–4.04 (m, J = 6.3 Hz, 2H, H-4′a and H-4′b), 4.18–4.24 (m, 1H, H-3′a), 4.64 (s, 2H, CH_2-C≡), 4.65 (d, 1H, H-1′b), 4.95–5.15 (m, 3H, H-2′a, OH-2′b and OH-3′b), 5.20 (br, 1H, OH-3′a), 5.45 (br, 1H, OH-2′a), 5.52 (dd, 1H, OH-5′), 5.97 (d, J = 6.8 Hz, 1H, H-1′a), 7.32 (br, 1H, $CONH_2$), 7.42 (t, J = 7.8 Hz, 1H, H Ph), 7.55 (d, 1H, H Ph), 7.64 (br, 2H, NH_2), 7.77 (d, 1H, H Ph), 7.86 (s, 1H, H Ph), 7.95 (br, 1H, $CONH_2$), 8.17 (s, 1H, H-2a); ^{13}C NMR (100 MHz, DMSO-d_6): δ 58.79 (***C***H_2-C≡), 62.64 (C-5′a), 71.29 (C-5′b), 71.45 (C-3′a), 72.07 (C-2′a and C-3′b), 75.58 (CH_2-***C*** ≡ C), 77.61 (C-2′b), 83.27 (C-4′b), 83.91 (C-1′b), 87.17 (C-4′a), 89.90 (C-1′a), 92.68 (CH_2-C ≡ ***C***), 119.83 (C-5), 126.03, 126.88, 128.53 and 129.37 (CH Ph), 133.48 (C-8), 134.67 and 141.58 (Cq Ph), 148.89 (C-4), 153.89 (C-2), 156.64 (C-6), 168.45 ($CONH_2$); HRMS (ESI$^+$-TOF): m/z calcd for $[C_{25}H_{28}N_6O_9 + H]^+$ 557.1991, found 557.1987.

Compound **1** was dissolved at 20 mM in dimethylsulfoxide (DMSO) 100%. For activity measurements, the stock solution was first diluted at 200 μM in DMSO and then further diluted in the experimental buffer at the indicated concentrations (final concentration of DMSO was kept constant at 5%). For bath infection, the stock solution was first diluted at 2 mM by adding phosphate buffered saline (PBS) drop by drop and then further diluted at the indicated concentration.

Cytotoxicity

The synthesized compounds were assayed for cytotoxicity on MRC-5 (human foetal lung fibroblasts) cells. The cells were cultured in Dulbecco's modified Eagle's medium (DMEM) supplemented with 25 mM glucose, 10% (v/v) serum, 1% penicillin/streptomycin and kept under 5% CO_2 at 37 °C. The cell viability was assessed using the CellTiter Glo kit from Promega (G7572) after 72-h incubation time using four concentrations of compounds (1, 10, 25 and 50 μM) in triplicate.

Bacterial growth curves

Overnight culture of PAO1 strain was diluted 1 : 10 in LB and grown until OD_{600} = 0.7 and further diluted to OD_{600} = 0.1. For bacterial growth curve, compound **1** solution was first diluted at 2 mM by adding LB:phosphate buffered saline (PBS) (75 : 25) and then diluted at the indicated concentration in 96-well plate by adding drop by drop 100 μL of bacteria suspension by well. The same protocol was done for DMSO with a first dilution to 10% in LB:PBS. Bacterial growth was monitored in 96-well plates by measuring the OD_{600} with a spectrophotometer (TECAN Spark®, Männedorf, Switzerland) during 6 h at 37 °C.

Experiments on zebrafish embryos

Bath infection of zebrafish embryos with *P. aeruginosa*

Experiments were performed using the GAB zebrafish line, which is maintained at 28 °C under standard conditions in fish water [43]. Preparation of bacteria and immersion infection of injured zebrafish embryos was realized as described [17] with the following modifications. All experiments were conducted on groups of 20 injured embryos into 96-well plates (two embryos per well) containing 200 μL of fish water supplemented with bacterial suspension and compound **1** or DMSO as control. The compound **1** stock solution was first diluted at 2 mM by adding PBS drop by drop. Bacterial suspension was then added drop by drop to compound **1** to reach a final concentration of 20 μM before immersion of injured embryos. Toxicity was addressed with non-infected injured embryos treated with compound **1**. For survival kinetics, the number of dead embryos was determined visually based on the absence of heartbeat.

Statistical analysis

Statistical analyses were performed using GRAPHPAD PRISM 5 (GraphPad Software, San Diego, CA, USA). Comparisons between survival curves were performed using the log-rank test.

Acknowledgements

This work was funded by the Agence Nationale de la Recherche (ANR-17-CE18-0011) and supported by Institut Pasteur, the Centre National de la Recherche Scientifique (CNRS), Institut National de la Santé et de la Recherche Médicale (INSERM) and University of Montpellier. R.R., P.N. and D.A.C. acknowledge ANR for financial support. The authors would like to thank the Chemogenomic and Biological Screening Platform (Institut Pasteur, France) for carrying out the cytotoxicity experiments and Frédéric Bonhomme (CNRS, UMR3523, Paris) for assisting with HRMS analysis. We thank Dr. Catherine Dunyach-Remy and Andréa Clary (INSERM U1047) for helpful discussion. We also acknowledge support from the French Infrastructure for Integrated Structural Biology (FRISBI) ANR-10-INSB-0005.

Conflict of interest

A patent on the molecule series described here and their applications have been deposited by INSERM Transfert on the 15 July 2022 under the reference EP22185280.9.

Author contributions

RR performed experiments, analysed data, prepared figures and wrote the paper. PN and DAC performed experiments, analysed data and prepared figs. VH and MG performed experiments and analysed data. GL and SP planned experiments, analysed data, prepared figures, wrote the paper and raised funds. ABBP planned experiments, analysed data, wrote the paper and raised funds. CL planned experiments, performed experiments, analysed data, prepared figures, wrote the paper and raised funds.

Ethics statement

All animal experiments described in the present study were conducted at the University of Montpellier according to European Union guidelines for handling of laboratory animals and were approved by the Direction Sanitaire et Vétérinaire de l'Hérault and Comité d'Ethique pour l'Expérimentation Animale under reference CEEA-LR- B4-172-37 and APAFIS#5737-2 016 061 511 212 601 v3.

Peer review

The peer review history for this article is available at https://publons.com/publon/10.1111/febs.16604.

References

1 Tacconelli E, Carrara E, Savoldi A, Harbarth S, Mendelson M, Monnet DL, et al. Discovery, research, and development of new antibiotics: the WHO priority list of antibiotic-resistant bacteria and tuberculosis. *Lancet Infect Dis*. 2018;**18**:318–27.
2 Gelin M, Poncet-Montange G, Assairi L, Morellato L, Huteau V, Dugué L, et al. Screening and in situ synthesis using crystals of a NAD kinase lead to a potent antistaphylococcal compound. *Structure*. 2012;**20**:1107–17.
3 Agledal L, Niere M, Ziegler M. The phosphate makes a difference: cellular functions of NADP. *Redox Rep*. 2010;**15**:2–10.
4 Pollak N, Dölle C, Ziegler M. The power to reduce: pyridine nucleotides – small molecules with a multitude of functions. *Biochem J*. 2007;**402**:205–18.
5 Grose JH, Joss L, Velick SF, Roth JR. Evidence that feedback inhibition of NAD kinase controls responses to oxidative stress. *Proc Natl Acad Sci USA*. 2006;**103**:7601–6.
6 Van Acker H, Coenye T. The role of reactive oxygen species in antibiotic-mediated killing of bacteria. *Trends Microbiol*. 2017;**25**:456–66.
7 Gerdes SY, Scholle MD, D'Souza M, Bernal A, Baev MV, Farrell M, et al. From genetic footprinting to antimicrobial drug targets: examples in cofactor biosynthetic pathways. *J Bacteriol*. 2002;**184**:4555–72.
8 Thanassi JA, Hartman-Neumann SL, Dougherty TJ, Dougherty BA, Pucci MJ. Identification of 113 conserved essential genes using a high-throughput gene disruption system in *Streptococcus pneumoniae*. *Nucleic Acids Res*. 2002;**30**:3152–62.
9 Zalacain M, Biswas S, Ingraham KA, Ambrad J, Bryant A, Chalker AF, et al. A global approach to identify novel broad-spectrum antibacterial targets among proteins of unknown function. *J Mol Microbiol Biotechnol*. 2003;**6**:109–26.
10 Kobayashi K, Ehrlich SD, Albertini A, Amati G, Andersen KK, Arnaud M, et al. Essential *Bacillus subtilis* genes. *Proc Natl Acad Sci USA*. 2003;**100**:4678–83.
11 Sassetti CM, Boyd DH, Rubin EJ. Genes required for mycobacterial growth defined by high density mutagenesis. *Mol Microbiol*. 2003;**48**:77–84.
12 Spaans SK, Weusthuis RA, van der Oost J, Kengen SWM. NADPH-generating systems in bacteria and archaea. *Front Microbiol*. 2015;**6**:742.
13 Poncet-Montange G, Assairi L, Arold S, Pochet S, Labesse G. NAD kinases use substrate-assisted catalysis for specific recognition of NAD. *J Biol Chem*. 2007;**282**:33925–34.
14 Labesse G, Douguet D, Assairi L, Gilles AM. Diacylglyceride kinases, sphingosine kinases and NAD

kinases: distant relatives of 6-phosphofructokinases. *Trends Biochem Sci*. 2002;**27**:273–5.
15 Paoletti J, Assairi L, Gelin M, Huteau V, Nahori M-A, Dussurget O, et al. 8-thioalkyl-adenosine derivatives inhibit *Listeria monocytogenes* NAD kinase through a novel binding mode. *Eur J Med Chem*. 2016;**124**: 1041–56.
16 Gelin M, Paoletti J, Nahori M-A, Huteau V, Leseigneur C, Jouvion G, et al. From substrate to fragments to inhibitor active in vivo against *Staphylococcus aureus*. *ACS Infect Dis*. 2020;**6**:422–35.
17 Nogaret P, El Garah F, Blanc-Potard A-B. A novel infection protocol in zebrafish embryo to assess *Pseudomonas aeruginosa* virulence and validate efficacy of a quorum sensing inhibitor in vivo. *Pathogens*. 2021;**10**:401.
18 Pont S, Blanc-Potard A-B. Zebrafish embryo infection model to investigate *Pseudomonas aeruginosa* interaction with innate immunity and validate new therapeutics. *Front Cell Infect Microbiol*. 2021;**11**:745851.
19 Li B-B, Wang X, Tai L, Ma T-T, Shalmani A, Liu W-T, et al. NAD kinases: metabolic targets controlling redox co-enzymes and reducing power partitioning in plant stress and development. *Front Plant Sci*. 2018;**9**:379.
20 Garavaglia S, Galizzi A, Rizzi M. Allosteric regulation of *Bacillus subtilis* NAD kinase by quinolinic acid. *J Bacteriol*. 2003;**185**:4844–50.
21 Orsak T, Smith TL, Eckert D, Lindsley JE, Borges CR, Rutter J. Revealing the allosterome: systematic identification of metabolite-protein interactions. *Biochemistry*. 2012;**51**:225–32.
22 Kawai S, Mori S, Mukai T, Hashimoto W, Murata K. Molecular characterization of *Escherichia coli* NAD kinase: *E. coli* ATP-NAD kinase. *Eur J Biochem*. 2001;**268**:4359–65.
23 Shi F, Huan X, Wang X, Ning J. Overexpression of NAD kinases improves the L-isoleucine biosynthesis in *Corynebacterium glutamicum* ssp. *lactofermentum*. *Enzyme Microb Technol*. 2012;**51**:73–80.
24 London J, Knight MY. Concentrations of nicotinamide nucleotide coenzymes in micro-organisms. *Microbiology*. 1966;**44**:241–54.
25 Krissinel E, Henrick K. Inference of macromolecular assemblies from crystalline state. *J Mol Biol*. 2007;**372**:774–97.
26 Mary C, Soflaee MH, Kesavan R, Gelin M, Brown H, Zacharias G, et al. Crystal structure of human NADK2 reveals a dimeric organization and active site occlusion by lysine acetylation. *Mol Cell*. 2022;**82**:3299–3311.e8.
27 Krohn K, Heins H, Wielckens K. Synthesis and cytotoxic activity of C-glycosidic nicotinamide riboside analogues. *J Med Chem*. 1992;**35**:511–7.
28 Pankiewicz KW, Zeidler J, Ciszewski LA, Bell JE, Goldstein BM, Jayaram HN, et al. Synthesis of isosteric analogues of nicotinamide adenine dinucleotide containing C-nucleotide of nicotinamide or picolinamide. *J Med Chem*. 1993;**36**:1855–9.
29 Franchetti P, Cappellacci L, Perlini P, Jayaram HN, Butler A, Schneider BP, et al. Isosteric analogues of nicotinamide adenine dinucleotide derived from furanfurin, thiophenfurin, and selenophenfurin as mammalian inosine monophosphate dehydrogenase (type I and II) inhibitors. *J Med Chem*. 1998;**41**: 1702–7.
30 Bonnac L, Chen L, Pathak R, Gao G, Ming Q, Bennett E, et al. Probing binding requirements of NAD kinase with modified substrate (NAD) analogues. *Bioorg Med Chem Lett*. 2007;**17**:1512–5.
31 Pankiewicz KW, Petrelli R, Singh R, Felczak K. Nicotinamide adenine dinucleotide based therapeutics, update. *Curr Med Chem*. 2015;**22**:3991–4028.
32 Rennekamp AJ, Peterson RT. 15 years of zebrafish chemical screening. *Curr Opin Chem Biol*. 2015;**24**:58–70.
33 Zon LI, Peterson RT. *In vivo* drug discovery in the zebrafish. *Nat Rev Drug Discov*. 2005;**4**:35–44.
34 Eimon PM, Rubinstein AL. The use of *in vivo* zebrafish assays in drug toxicity screening. *Expert Opin Drug Metab Toxicol*. 2009;**5**:393–401.
35 Gomes MC, Mostowy S. The case for modeling human infection in zebrafish. *Trends Microbiol*. 2020;**28**: 10–8.
36 Clément DA, Leseigneur C, Gelin M, Coelho D, Huteau V, Lionne C, et al. New chemical probe targeting bacterial NAD kinase. *Molecules*. 2020;**25**: E4893.
37 Pergolizzi G, Butt JN, Bowater RP, Wagner GK. A novel fluorescent probe for NAD-consuming enzymes. *Chem Commun (Camb)*. 2011;**47**:12655–7.
38 Depaix A, Kowalska J. NAD analogs in aid of chemical biology and medicinal chemistry. *Molecules*. 2019;**24**:E4187.
39 Manalastas-Cantos K, Konarev PV, Hajizadeh NR, Kikhney AG, Petoukhov MV, Molodenskiy DS, et al. ATSAS 3.0: expanded functionality and new tools for small-angle scattering data analysis. *J Appl Cryst*. 2021;**54**:343–55.
40 Franke D, Petoukhov MV, Konarev PV, Panjkovich A, Tuukkanen A, Mertens HDT, et al. ATSAS 2.8: a comprehensive data analysis suite for small-angle scattering from macromolecular solutions. *J Appl Cryst*. 2017;**50**:1212–25.
41 Vonrhein C, Keller P, Smart O, Womack T, Bricogne G. Data processing and analysis with the autoPROC toolbox. *Acta Crystallogr D Biol Crystallogr*. 2011;**67**:293–302.

42 Catherinot V, Labesse G. ViTO: tool for refinement of protein sequence-structure alignments. *Bioinformatics*. 2004;**20**:3694–6.
43 Belon C, Soscia C, Bernut A, Laubier A, Bleves S, Blanc-Potard A-B. A macrophage subversion factor is shared by intracellular and extracellular pathogens. *PLoS Pathog*. 2015;**11**:e1004969.
44 Robert X, Gouet P. Deciphering key features in protein structures with the new ENDscript server. *Nucleic Acids Res*. 2014;**42**:W320–4.

Supporting information

Additional supporting information may be found online in the Supporting Information section at the end of the article.

Appendix S1. NMR spectra of the original compounds synthesized here.